CHARACTERIZATION AND BIOLOGICAL ANALYSIS OF β-DICALCIUM SILICATE/DICALCIUM PHOSPHATE-BASED CEMENT FOR DENTAL APPLICATIONS

2024
MASTER THESIS
BIOMEDICAL ENGINEERING

Almataz Bellah MARANDI

Thesis Advisors
Assoc.Prof.Dr. Daver ALI
Assist.Prof.Dr. Ammar ZIDANOGLU

CHARACTERIZATION AND BIOLOGICAL ANALYSIS OF β-DICALCIUM SILICATE/DICALCIUM PHOSPHATE-BASED CEMENT FOR DENTAL APPLICATIONS

Almataz Bellah MARANDI

Thesis Advisors
Assoc. Prof. Dr. Daver ALI
Assist. Prof. Dr. Ammar ZIDANOGLU

T.C.
Karabuk University
Institute of Graduate Programs
Department of Bıomedıcal Engıneerıng
Prepared as
Master Thesis

KARABUK
June 2024

I certify that in my opinion the thesis submitted by Almataz Bellah MARANDI titled "CHARACTERIZATION AND BIOLOGICAL ANALYSIS OF β-DICALCIUM SILICATE/DICALCIUM PHOSPHATE-BASED CEMENT FOR DENTAL APPLICATIONS " is fully adequate in scope and in quality as a thesis for the degree of Master of Science.

Assoc.Prof.Dr. Daver ALI .....
Thesis Advisor, Department of Biomedical Engineering

Assist.Prof.Dr. Ammar ZIDANOĞLU .....
2. Thesis Advisor, Department of Biomedical Engineering

This thesis is accepted by the examining committee with a unanimous vote in the Department of Biomedical Engineering as a Master of Science thesis. 27.06.2024

Examining Committee Members (Institutions)	Signature
Chairman : Assist.Prof.Dr. Khaled M.N. CHAHROUR (KBU)	.....
Member : Assoc.Prof.Dr. Daver ALI (KBU.)	.....
Member : Assist.Prof.Dr. İsmail SEÇKİN (ATAU)	.....

The degree of Master of Science by the thesis submitted is approved by the Administrative Board of the Institute of Graduate Programs, Karabuk University.

Assoc. Prof. Dr. Zeynep ÖZCAN .....
Director of the Institute of Graduate Programs

"I declare that all information contained in this document has been obtained and presented in accordance with academic rules and ethics. i also declare that, in accordance with these rules and conduct, i have cited and referenced all non-original material and results in this document"

Almataz Bellah MARANDI

ABSTRACT

M. Sc. Thesis

CHARACTERIZATION AND BIOLOGICAL ANALYSIS OF β-DICALCIUM SILICATE/DICALCIUM PHOSPHATE-BASED CEMENT FOR DENTAL APPLICATIONS

Almataz Bellah MARANDI

Karabuk University
Institute of Graduate Programs
Department of Biomedical Engineering

Thesis Advisors:
Assoc. Prof. Dr. Daver ALI
Assist. Prof. Dr Ammar ZIDANOĞLU
June 2024, 66 pages

This study focuses on synthesizing and characterizing β-Dicalcium silicate (β-C_2S) and Dicalcıum phosphate (DCP)-based composite cements for dental and orthopedic applications. The primary objective is to develop a composite material that balances antibacterial efficacy, cytocompatibility, and mechanical strength. β-C_2S and DCP were synthesized using sol-gel and microwave-assisted wet precipitation methods, respectively. The resulting cements were characterized using X-ray Diffraction (XRD), Fourier-transform infrared spectroscopy (FTIR), Scanning Electron Microscopy (SEM), and Thermogravimetric analysis (TGA).

XRD analysis confirmed the successful synthesis of pure β-C_2S and DCP phases with no detectable contaminants. SEM images revealed that pure DCP particles exhibited a plate-like structure, while the addition of β-C_2S resulted in a more cross-

linked and fibrous microstructure. FTIR spectra identified characteristic peaks corresponding to the chemical bonds in the composite cements. TGA indicated that the composite cements exhibited improved thermal stability compared to pure DCP.

Mechanical testing showed that the compressive strength of the composite cements increased with the β-C_2S content, reaching up to 8.19 MPa for the 40% β-C_2S /DCP composite, which is comparable to human cancellous bone. Antibacterial activity tests against Staphylococcus aureus (S. aureus) demonstrated that pure DCP cement loaded with Gentamicin had the highest antibacterial efficacy, while the addition of β-C_2S reduced bacterial growth to varying degrees. Cytocompatibility studies using Saos-2 cell lines indicated that the 20% β-C_2S /DCP composite supported the highest cell viability, with optimal pH levels contributing to enhanced cell growth.

Overall, the β-C_2S /DCP composite cements exhibit promising properties for potential use in dental applications, offering a balanced combination of mechanical strength, antibacterial activity, and biocompatibility. Further optimization and in vivo studies are recommended to fully realize the clinical potential of these composite materials.

Key Words **:** Dicalcium phosphate cement; β-dicalcium silicate; Mechanical strength; Antibacterial activity; Biocompatibility.

Science Code **:** 92503

ÖZET

Yüksek Lisans Tezi

DİŞÇİLİK UYGULAMALARINA YÖNELİK β-DİKALSİYUM SİLİKAT/DİKALSİYUM FOSFAT BAZLI ÇİMENTOLARIN KARAKTERİZASYONU VE BİYOLOJİK ANALİZİ

Almataz Bellah MARANDI

Karabük Üniversitesi
Lisansüstü Eğitim Enstitüsü
Biyomedikal Mühendisliği Anabilim Dalı

Tez Danışmanları:
Doç. Dr. Daver ALI
Dr. Öğr. Üyesi Ammar ZIDANOĞLU
Haziran 2024, 66 sayfa

Bu çalışmada dikalsiyum fosfat (DCP) çimentosu ve onun β-dikalsiyum silikat (β-C_2S) ile kompozitlerinin sentezi ve karakterizasyonu araştırılmıştır. Saf DCP çimentosu ve %20, %30 ve %40 β-C_2S içeren kompozitler çeşitli teknikler kullanılarak hazırlanıp analiz edildi. X-ışını kırınımı testi sonucunda, çimentolarda bruşit ve monetit fazlarının oluşumu doğruladı. Termogravimetrik analizle, saf DCP, %20 β-C_2S/DCP, %30 β-C_2S/DCP ve %40 β-C_2S/DCP için sırasıyla %21,205, %17,368, %11,576 ve %15,890 ağırlık kaybının olduğu görülmüştür. Basınç dayanımı testi %40 β-C_2S/DCP için 8,19 MPa olarak hesaplanmıştır ki bu dayanıklık insan süngerimsi kemiğin basınç dayanımına yakındır. Staphylococcus aureus'a karşı antibakteriyel aktivite, 100 mg/ml konsantrasyonda saf DCP için en yüksek düzeydeydi ancak β-C_2S ilavesiyle azaldı. Saos-2 hücreleriyle yapılan hücre kültürü

çalışmaları, 4 ve 7 gün sonra özellikle %20 ve %40 konsantrasyonlarda β-C_2S eklenmesiyle canlılık oranın arttığını gösterdi. Kültür ortamının pH'ı β-C_2S/DCP kompozitleri için 7-8'de sabit kalırken, saf DCP bunu 6 olarak ölçüldü. Bu sonuçlar, özellikle %40 β-C_2S içeriğinde β-C_2S/DCP kompozitlerinin gelişmiş özellikler sunduğunu göstermektedir. Bu çalışmada saf DCP çimentoya kıyasla %40 β-C_2S içeriğinde β-C_2S/DCP'ın mekanik ve biyouyumluluk açısından daha iyi olup ve onları diş ve ortopedik uygulamalar için umut verici malzemeler olduğu görülmektedir.

Anahtar Sözcükler : Dikalsiyum fosfat çimentosu; β-dikalsiyum silikat; Diş hamuru çimentosu; Karakterizasyonlar

Bilim Kodu : 920503

ACKNOWLEDGEMENT

I express my sincere gratitude to Assist. Prof. Dr Ammar ZIDANOĞLU for granting my request to work under his guidance and for his continuous support, timely interventions, and valuable counsel during the course of my project, which ultimately resulted in its successful completion. His amiable demeanor rendered him a readily accessible mentor, fostering both professional collaboration and personal rapport.

I also extend my heartfelt thanks to Assoc. Prof. Dr. Daver ALI and Assist. Prof. Dr Ali Deniz DALGIÇ for their significant contributions to the success of this thesis. I am deeply grateful to the Biomaterials Laboratory, Department of Engineering Sciences at Middle East Technical University, for generously providing the essential resources required to successfully complete this thesis.

My profound appreciation goes to my parents for their unwavering support and invaluable contributions throughout my life and academic pursuits. I am also deeply thankful to my family and sisters for their great assistance during my thesis study.

CONTENTS

Page

Page

Page

LIST OF FiGURES

Page

LIST OF TABLES

Page

SYMBOLS AND ABBREVIATIONS

SYMBOLS

°	Degree
°C	The degree Celsius
Å	Angstrom
µL	Microliter
3D	Three Dimensional
C	Carbon
N	Nitrogen
H	Hydrogen
O	Oxygen
P	Phosphorus
Ca	Calcium
cm	Centimeter
nm	Nanometer
Dth	Theoretical density
g	Gram
kg	Kilogram
*I*a	Monoclinic space group
kN	Kilonewton
L	Liter
mL	milliliter

MPa	Megapascal
*P*1	Triclinic space group
P21/a	Monoclinic space group
P63/mmc	Hexagonal space group
R3c	Rhombohedral space group
rpm	Revolutions per minute
sec	Second
V	Cell volume
V_0	Volume per formula unit
Z	Number of formula units per cell
W	Watt
α	Alpha, cell angle
β	Beta, cell angle
γ	Gamma, cell angle
2θ	The diffraction angle

ABBREVIATIONS

ASTM	American Society for Testing and Materials
JCPDS	Joint Committee on Powder Diffraction and Standards
CPs	Calcium Phosphates
MCPM	Mono Calcium Phosphate Monohydrate
TCP	Tricalcium Phosphate
DCP	Dicalcium Phosphate
DCPA	Dicalcium Phosphate Anhydrous
DCPD	Dicalcium Phosphate Dihydrate
C_2S	Dicalcium Silicate
DPSCs	Dental Pulp Stem Cells
β-$Ca_2P_2O_7$	β-calcium pyrophosphate
HA	Hydroxyapatite
FDA	American Food and Drug Administration
FTIR	Fourier Transform Infrared Spectroscopy
SBF	Simulated Body Fluid
SEM	Scanning Electron Microscopy
TGA	Thermo Gravimetric Analysis
XRD	X-Ray Diffraction
α-TCP	α - Tricalcium Phosphate
α′-TCP	α′ - Tricalcium Phosphate
β-TCP	β - Tricalcium Phosphate

CHAPTER 1

INTRODUCTION

1.1.TEETH STRUCTURE

Tissue engineering in dentistry has been rapidly evolving due to advancements in biomedical technology. Regenerative medicine is critical in dentistry, particularly in tooth and pulp regeneration [1]. Tooth or dental tissue loss can result from a variety of causes, including trauma, dental caries, periodontal disease, severe injury, medical conditions, and inherited disorders. This widespread and chronic health issue can significantly impact an individual's quality of life [2]. Dentists employ a range of dental restorative materials in various treatments to repair teeth and alleviate pain. A substantial portion of dental research is dedicated to developing and improving dental materials, particularly bioactive restorative dental applications. These bioactive materials replace damaged or lost tissue and interact with the surrounding environment to promote healing and regeneration [3–6]. Before delving into the technical aspects of dental biomaterials, it is essential to understand tooth anatomy (Figure 1.1) [7]. The basic structure of a tooth consists of four main components: enamel, dentin, cementum, and pulp. The enamel is the hardest tissue in the human body and forms the outer layer of the tooth crown. Beneath the enamel lies dentin, which makes up the bulk of the tooth and extends from the crown to the root. The cementum covers the root surface, while the pulp in the center of the tooth contains nerves, blood vessels, and connective tissue.

Understanding dental anatomy is crucial for developing effective bioactive materials that mimic natural tooth structure and function. As research in this field progresses, it holds great promise for improving dental treatments and outcomes for patients with tooth loss or damage.

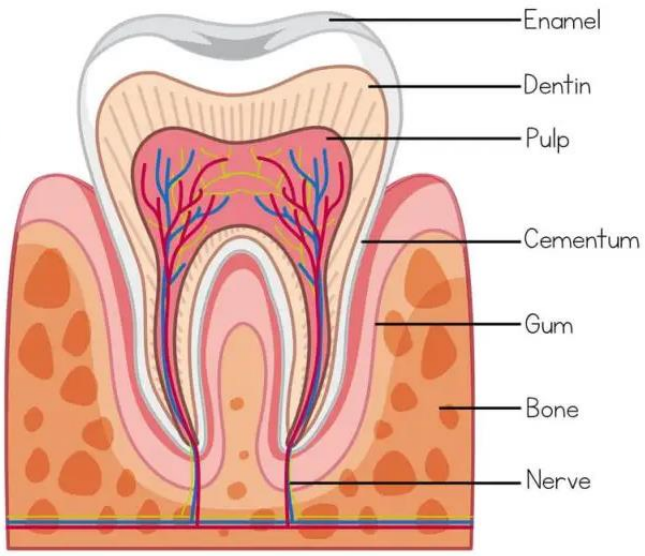

Figure 1.1. Structure of the tooth [7].

The human dentition consists of 32 permanent teeth and 20 primary (deciduous) teeth that are eventually replaced [7,8]. Enamel, dentin, cementum, and dental pulp, all specialized mineralized tissues except for the pulp, compose each tooth [7,9–11]. The tooth's crown, covered by enamel, protects the internal pulp chamber and roots [7,10]. During tooth development, the neural crest contributes to dentin, pulp, and gingiva formation while the oral epithelial tissue forms the enamel [7,9]. Dentin, the primary component of teeth, is a mineralized tissue composed of collagen and minerals. Its chemical composition is similar to bone but with a higher degree of mineralization, making it harder. Dentin plays a crucial role in the metabolic processes of enamel and cementum [12,13]. It comprises approximately 70% inorganic compounds, primarily hydroxyapatite and calcium carbonate, amorphous phosphate, magnesium ions, and trace metals. The organic components are about 20% dentin, with 90% type I collagen. The remaining 10% is water [12,14]. Cementum, a mineralized substance surrounding the tooth root, has a composition similar to that of bone. It comprises 50–55% organic constituents (including collagen, non-collagenous proteins, proteoglycans, glycoproteins, and phosphoproteins) and 45–50% inorganic substances (primarily hydroxyapatite) and water. Cementum formation continues throughout life, beginning with the emergence of permanent teeth. Due to its avascular nature, it rarely undergoes

remodeling or resorption [12–14]. The dental pulp, a soft connective tissue rich in blood vessels and nerves, resides within the tooth. It comprises various cell types interconnected by a network of collagen fibers. The pulp's primary functions include dentin production, nourishment of adjacent mineralized tissue, self-protection and repair when injured, and contribution to tooth sensitivity. Encased within rigid dental tissues, the pulp is divided into several distinct zones [15].

1.2.CEMENTS AS DENTAL REPAIR MATERIALS

Active biomaterials are increasingly preferred over passive and inert ones for tissue regeneration. These materials, often referred to as bioactive materials, have the capacity to interact with biological systems and promote tissue healing. They have various applications in dentistry, including bonding, dental cementation, pulp capping, and restorative materials [4,5]. Implant fixation and other dental procedures commonly use dental cements. Typically, a chemical reaction between powder and liquid components forms them, resulting in an intermediate phase of paste. Once placed in the body, these cements self-set and solidify [16–18].

Materials can be classified as polymeric, ceramic, composite, or metallic based on their fundamental chemistry [5,19]. This study focuses on ceramic materials, specifically bioceramics. A bioceramic is a nonmetallic, inorganic, and biocompatible material designed to replace or repair tough tissues, possessing mechanical properties similar to those of natural tough tissues. Bioceramics interact favourably with organic tissues, are non-corrosive, and are chemically stable [8]. Ceramic materials can be further categorized into oxide and non-oxide types.

Bioceramic materials have gained popularity over the past two decades due to their potential to enhance physiological function and form strong bonds with hard tissues [8]. However, it's important to note that no perfect cement currently exists in the medical field, as all ceramic biocements have certain limitations [20]. An ideal dental cement should possess several key characteristics, including thin coating thickness, minimal solubility, no micro-leakage, low viscosity, strength and hardness comparable to dentin, and adequate working time. Additionally, the material must be

biocompatible and possess antimicrobial properties to prevent potential infections or harm to the user [21,22].

1.2.1. Dicalcium Phosphate Cements

Dicalcium Phosphate (DCP) cement possesses qualities that make it well-suited for various therapeutic applications, particularly in bone replacement. Its favourable features include osteoconductivity, bioactivity, formability, and injectability. DCP is particularly well-suited for a wide range of surgical procedures, including dental and maxillofacial applications and areas of the body affected by osteonecrosis. This versatility is due to its exceptional formability and low setting temperature, making it an ideal choice for such applications [9,23–25]. The ability of DCP to form when combined with various compounds is an essential attribute to consider [8,24,26].

Additionally, DCP can be an effective carrier for drugs and biomolecules [24]. However, it has some limitations, notably subpar mechanical characteristics and a slow degradation rate. To address these issues, researchers have employed various materials, such as chitin, cellulose, chitosan, alginate, collagen, and synthetic polymers, to enhance the degradation rate and mechanical properties of DCP [9]. Recent studies have shown that combining dicalcium phosphate with calcium silicate can improve the properties above [27,28]. This combination has demonstrated potential for supporting and enhancing the desirable characteristics of DCP, making it an even more promising material for bone replacement and regeneration applications. By addressing the limitations of DCP while maintaining its beneficial properties, researchers aim to develop more effective and versatile bone cement formulations. These improvements could lead to better outcomes in various surgical procedures and expand the potential applications of DCP in regenerative medicine and tissue engineering [27,28].

1.2.2. Dicalcium Silicate Cements

Many calcium silicate-based cements have been reported for use in bone substitute applications and dental procedures, with some demonstrating remarkable performance in both in vitro and in vivo osteogenesis and odontogenesis [26]. Dicalcium Silicate (C_2S), also known as larnite or belite, is an essential mineral with distinct features such as non-toxic bioactivity, exceptional thermal and chemical stability, high energy storage capacity, and flame resistance [29,30]. Recent research indicates that the beta polymorph of β- Dicalcium Silicate (β-C_2S) has significant potential in dentistry. β-C_2S cement possesses excellent biological properties, making it suitable as both a root-end filling material and a pulp-capping agent. Its bioactivity and biocompatibility have been well-documented in vitro [31–33].

Additionally, β-C_2S cement has a high capacity to form apatite and demonstrates durability in acidic conditions, which is advantageous for root-end filling applications. Furthermore, β-C_2S cement may serve as an effective model system for drug delivery [34,35]. Heating dicalcium silicate releases silicon ions, crucial for bone formation and repair [36]. The study results provide compelling evidence for the widespread use of β-C_2S cement, highlighting its potential for a wide array of orthopedic and dental applications in the future.

1.3. PROBLEM STATEMENT

The development of DCP/β-C_2S composite cement aims to combine the beneficial properties of both materials for dental and orthopedic applications. However, optimizing the composition and properties of these composite cements presents several challenges. Pure DCP cement exhibits mechanical strength and biocompatibility limitations, necessitating modifications to enhance its performance. The addition of β-C_2S to DCP cement alters its microstructure, setting behaviour, and biological properties, but the optimal ratio and its effects on cement properties are not fully understood. There is a need to carefully balance these composite cements' antibacterial activity, cytocompatibility, and mechanical strength. The slow hydration rate of β-C_2S could affect how strong the composites become early on, limiting their ability to hold

weight right away. Additionally, optimizing the synthesis methods, particle size distribution, and setting reactions of these composite cements to achieve desired handling properties and biological responses remains an ongoing challenge in bioactive cement development for dental and orthopedic uses [10,11].

1.4. THESIS OBJECTIVES

The objectives of this study can be summarised as follows:

- To synthesize and characterize β-tricalcium phosphate (β-TCP), β- C_2S, pure DCP cement (using β-TCP as a precursor), and DCP composite cements containing 20%, 30%, and 40% (β-C_2S), the following procedures will be employed:
  - ✓ Synthesis of individual components (β-TCP and β-C_2S).
  - ✓ Preparation of pure DCP cement.
  - ✓ Formulation of DCP composite cements with varying β-C_2S content.
  - ✓ The obtained cements will then be characterized using the following analytical techniques: (XRD) for phase identification and crystallinity analysis and Fourier-transform infrared spectroscopy (FTIR) for chemical bond identification. (SEM) for morphological examination. Thermogravimetric analysis (TGA) for thermal stability and composition assessment.
- To evaluate the antibacterial activity of the prepared cements loaded with gentamicin sulphate against Staphylococcus aureus (*S. aureus*) at different concentrations.
- To assess the cytocompatibility of the prepared cements by analyzing the viability and growth of osteosarcoma (Saos-2) cell lines when exposed to the cement samples over different periods.
- To investigate the effect of β-C2S addition on the mechanical properties, particularly the compressive strength, of the DCP-based cements.
- To determine the optimal composition of β-C2S/DCP composite cement that balances antibacterial efficacy, cytocompatibility, and mechanical strength for potential dental and orthopedic applications.

These objectives aim to comprehensively evaluate the properties and potential of β-C_2S/DCP composite cements for biomedical applications, focusing on their structural characteristics, antimicrobial activity, biocompatibility, and mechanical performance.

1.5.SIGNIFICANT OF THE THESIS

This thesis is significant because it has the potential to advance the field of biomedical engineering, particularly in developing dental and orthopedic cements. This study looks into how to make and characterize DCP and β-C_2S composite cements. It aims to find the best balance between their ability to kill bacteria and work with cells and their strength. The findings could create more effective and biocompatible materials for dental and bone regeneration applications, ultimately improving patient outcomes. The study's insights into composite cement's microstructural and chemical properties contribute to a broader understanding of material science, potentially influencing future innovations in bioactive and antibacterial materials.

CHAPTER 2

LITERATURE REVIEW

2.1. CALCIUM PHOSPHATES

Calcium phosphates (CPs) are a family of minerals that closely resemble the inorganic components of bones and teeth. Biomedical applications widely use them, especially in bone grafting and dental procedures, because of their biocompatibility and resemblance to natural bone. People often categorize calcium phosphates based on their calcium-to-phosphorus (Ca/P) molar ratio. This ratio is critical because it influences properties like solubility, acidity, and biological behaviour. A table summarizes common CPs (Table 2.1) [12].

Table 2.1. Main cps types [14,37–39].

Name	Ca/P ratio	Symbol	Formula	Mineral
Monocalcium phosphate monohydrate	0.50	MCPM	$Ca(H_2PO_4)_2 \cdot H_2O$	-
Monocalcium phosphate	0.50	MCP	$Ca(H_2PO_4)_2$	-
Dicalcium phosphate	1.00	DCP	$CaHPO_4$	Monetite
Dicalcium phosphate dihydrate	1.00	DCPD	$CaHPO_4 \cdot H_2O$	Brushite
Octocalcium phosphate	1.33	OCP	$Ca_3H_2(PO_4)_6 \cdot 5H_2O$	-
Sintered hydroxyapatite	1.67	SHA	$Ca_{10}(PO_4)_6(OH)_2$	Hydroxy apatite
β-Tricalcium phosphate	1.50	β-TCP	$\beta\text{-}Ca_3(PO_4)_2$	-
α-Tricalcium phosphate	1.50	α-TCP	$\alpha\text{-}Ca_3(PO_4)_2$	-
Oxyapatite	1.67	OXA	$Ca_{10}(PO_4)_6O$	-

2.1.1. Monocalcium Phosphate Monohydrate

Monocalcium phosphate monohydrate (MCPM), with the chemical formula $Ca(H_2PO_4)_2 \cdot H_2O$, is a highly soluble compound that significantly lowers the pH of water when dissolved, maintaining phase stability at pH levels below 2 [40]. Due to its high acidity and solubility, MCPM is not involved in biological mineralization processes and demonstrates poor compatibility with bone tissue [41]. When MCPM is subjected to a drying process at 100°C, the water molecules evaporate, forming an anhydrous form known as monocalcium phosphate anhydrous (MCPA), which has a higher density. DCP cements, widely used in dentistry, drug delivery, and various biological applications, are often derived from MCPM. These cements are biocompatible and bioactive, making them suitable for bone repair materials. While MCPM is unsuitable for direct biological applications due to its high acidity and solubility, its derivatives, particularly DCP cements, play a significant role in various biomedical fields. The transformation of MCPM to MCPA and its use in DCP cements underscore its importance in developing biocompatible materials for medical use [12,42,43].

2.1.2. Tricalcium Phosphate

Tricalcium phosphate (TCP), with the chemical formula $Ca_3(PO_4)_2$, is a versatile inorganic biomaterial widely used in biomedical applications such as coatings for metallic implants and bone defect repair, owing to its excellent biocompatibility, osteoconductivity, and bioactive properties [44,45]. Three types of TCP exist, and each is stable at a different temperature range (Table 2.2): β-TCP is rhombohedral and stable up to 1120–1125°C; α-TCP is monoclinic and stable between 1120–1125°C and 1430–1470°C; and α′-TCP is hexagonal and stable above 1430–1470°C. The phase transitions occur from β-TCP to α-TCP at 1120–1125 °C and from α-TCP to α′-TCP at 1430–1470 °C. β-TCP is the most commonly used form in biomedical applications due to its lower solubility and better biological resorbability compared to hydroxyapatite. Calcium phosphate cements often use α-TCP, which is more soluble and reactive in aqueous environments. α′-TCP has limited practical applications. Recent research has focused on improving TCP properties through ion substitutions

and developing composite materials to enhance biological performance and mechanical properties for bone regeneration applications. The synthesis and processing methods of TCP materials significantly influence their properties and performance, allowing for tailored particle size, specific surface area, and crystallinity to optimize their efficacy in various clinical settings [46–48].

Table 2.2. Structural information on the polymorphs of TCP [48,49].

Property	**TCP Polymorphs**		
	β-TCP	**α-TCP**	**α′-TCP**
Symmetry	Rhombohedral	Monoclinic	Hexagonal
Space group	R_3C	$P2_1/a$	$P6_3/mmc$
***a* (nm)**	1.04352	1.2859	0.53507
***b* (nm)**	1.04352	2.7354	0.53507
***c* (nm)**	3.74029	1.5222	0.7684
α (°)	90	90	90
β (°)	90	126.35	90
γ (°)	120	90	120
Z	21	24	1
***V* (nm^3)**	3.5272	4.31	0.19052
***V*$_0$ (nm^3)**	0.1680	0.180	0.19052
***D*$_{th}$ (g cm^{-3})**	3.066	2.866	2.702

2.1.2.1. β - Tricalcium Phosphate

β-Tricalcium phosphate (β-TCP), chemically represented as β-$Ca_3(PO_4)_2$, is a highly sought-after biomaterial for bone regeneration applications due to its excellent biocompatibility and osteoconductive properties [49,50]. Its rhombohedral crystal structure, belonging to the R3c space group [49,51], is characterized by unit cell parameters of a = b = 10.4352 Å and c = 37.4029 Å, with angles α = β = 90° and γ = 120°, and a density of approximately 3.07 g/cm³. The structure consists of complex formations of tetrahedral phosphate centers interconnected with calcium ions via oxygen atoms. β-TCP's popularity in biomedical applications stems from its ability to

form microporous scaffolds that demonstrate impressive mechanical strength and promote cell proliferation. Biphasic calcium phosphates widely utilize TCP as a standalone material or component, offering it in various forms, such as solid or porous granules and scaffolds. The material's biodegradability and osteoconductivity make it particularly valuable in bone tissue engineering [48,49].

Recent research shows that β-TCP can influence blood clot structure by modulating fibrin polymerization, which may affect bone healing in experimental models. Additionally, releasing Ca^{2+} ions from β-TCP plays a crucial role in its biological activity, potentially influencing cellular responses and bone formation processes. The versatility of β-TCP allows for its use in various therapeutic applications, including dental and orthopedic procedures, where it can effectively support bone regeneration and integration with surrounding tissues.

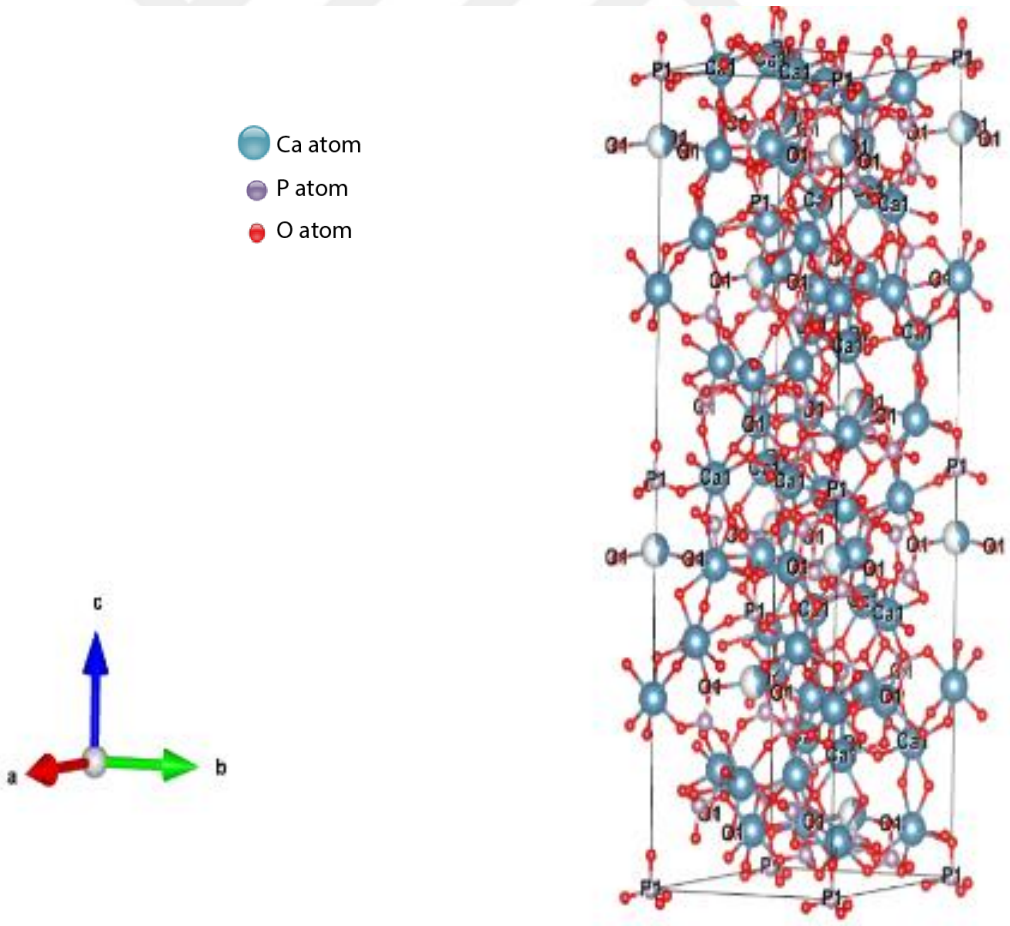

Figure 2.1. The unit cell structure of β-TCP.

Techniques for Producing β-TCP Particles

β-TCP is a crucial biomaterial in bone tissue engineering and regenerative medicine. Various techniques have been developed to synthesize β-TCP particles, each imparting distinct characteristics to the final product. The most common methods include wet chemical synthesis, the sol-gel approach, the hydrothermal method, microwave-assisted synthesis, and the solid-state reaction method [51–55].

I. Wet precipitation method

The wet precipitation method is widely used for synthesizing β-TCP due to its ability to control the composition and physical properties of the resulting powders. This process involves combining calcium (Ca^{2+}) and phosphate (PO_4^{3-}) precursors in a neutral or basic solution to produce low-crystallinity β-TCP [56]. The method offers several advantages: process simplicity, low-temperature synthesis, cost-effective raw materials, particle size and shape control, high purity, scalability, reproducibility, and flexibility in adjusting synthesis conditions. However, it faces challenges such as time-consuming production processes and potential phase purity issues due to the formation of calcium pyrophosphate ($Ca_2P_2O_7$) [57]. Recent developments have addressed these limitations through modifications like microwave-assisted synthesis, precise pH control, careful precursor selection, and post-synthesis treatments. Adding calcium pyrophosphate to porous β-TCP scaffolds can make them more brittle, which could be a good thing in some situations because it might break down more easily than β-TCP. Despite its challenges, the wet precipitation method remains a valuable tool in the development of advanced calcium phosphate-based biomaterials for bone tissue engineering and regenerative medicine applications, with ongoing research focusing on optimizing the process for specific uses and enhancing the properties of the resulting β-TCP materials [57,58].

II. Sol-gel method

The sol-gel method has garnered significant interest in synthesizing β-TCP due to its inherent advantages, such as uniform molecular blending, low-temperature operation, and the ability to produce nanocrystalline powders, bulk amorphous monolithic solids, and thin films [59]This process forms colloidal suspensions (sols) into gels, creating inorganic structures. When dried, the substance becomes a xerogel. The sol-gel method's simplicity, cost-effectiveness, and ability to control particle size and shape make it particularly attractive [60]. There are some problems with this method, though. For example, it needs expensive alkoxide-derived precursors and a lot of steps to fully dissolve the precursors and get phase-pure β-TCP after heat treatment. Therefore, there is a need to develop methodologies that are straightforward and can be easily executed without strict safeguards and meticulous manipulations [55,59,61]. There are several important steps in the sol-gel process. These are choosing the precursors, making sols through hydrolysis and polycondensation, gelation, aging, drying, and calcination at high temperatures. Recent advancements have focused on optimizing synthesis parameters, using alternative precursors, and incorporating additives to enhance the properties of the resulting β-TCP. For instance, researchers have explored microwave-assisted sol-gel synthesis to minimize processing times and energy consumption. Despite its challenges, the sol-gel method remains valuablen developing advanced calcium phosphate-based biomaterials for various biomedical applications, including bone tissue engineering and regenerative medicine [62].

III. Hydrothermal method

The hydrothermal method is a reliable and straightforward technique for synthesizing β-TCP, offering significant advantages such as reduced energy consumption and shorter reaction durations. This method allows for the precise control of nanostructure size and morphology by adjusting reaction conditions like pH, temperature, and pressure, distinguishing it from other synthesis approaches. Hydrothermal synthesis can produce large, high-quality crystals with excellent chemical uniformity, making it a preferred method for creating advanced materials [63]. Hydrothermal synthesis involves converting solutions or sols into crystalline phases under high-temperature

and high-pressure conditions, typically below 350 °C and 150 atm. This process enables the regulation of nucleation, growth, and maturation stages, allowing for the manipulation of particle size and shape [64–66]. By adjusting the pressure settings, which can be either high or low depending on the vapor pressure of the primary reactants, the morphology of the materials can be finely tuned [65,66]. This method is increasingly recognized as crucial for processing advanced materials, particularly nanostructural materials, in various technological applications. For instance, the hydrothermal method has successfully synthesized-TCP with high purity and controlled crystallinity, essential for biomedical applications such as bone grafts and tissue engineering scaffolds [67].

Recent advancements in hydrothermal synthesis have focused on optimizing experimental parameters to enhance the quality and properties of β-TCP. For example, studies have shown that increasing the reaction temperature and time can improve the crystallinity and phase purity of the resulting β-TCP. Researchers have also explored the integration of microwave energy in hydrothermal synthesis to reduce processing times further and enhance energy efficiency. The hydrothermal method's eco-friendly nature and ability to produce monodispersed nanoparticles with high dispersibility have made it popular in nanotechnology. Researchers have used it to synthesize a variety of advanced nanomaterials, such as metal oxides, semiconductors, and carbonaceous materials derived from biomass. In the context of TCP, hydrothermal synthesis produces materials with excellent osteoconductivity and biocompatibility, making them suitable for bone regeneration and repair.

The hydrothermal method is a flexible and effective way to make β-TCP. It has many benefits, such as using less energy, letting you control particle size and shape, and making high-quality materials that are chemically uniform. Ongoing research continues to refine this method, exploring new approaches and modifications to enhance the properties and performance of β-TCP for various biomedical and technological applications.

IV. Microwave-assisted wet precipitation method

The microwave-assisted wet precipitation method for synthesizing β-TCP offers a unique and efficient approach compared to conventional heating procedures. This technique utilizes electromagnetic waves, typically at a frequency of 2.45 GHz, to rapidly transmit energy directly to the reaction mixture, resulting in internal heating and a more uniform temperature distribution. The method's key principles include direct energy transfer to water molecules in the hydration sphere, uniform heating as the sample acts as its heat source, and rapid crystallization due to efficient energy transfer. These characteristics lead to several advantages, such as reduced reaction time, enhanced product purity, improved control over reaction conditions, and increased energy efficiency [17,68,69]. Recent advancements have demonstrated the versatility of this method, including green synthesis using waste materials, the production of high-purity β-TCP nanoparticles with controlled size and morphology, and the development of microwave-assisted solution combustion synthesis [68–70]. However, the technique also faces some limitations, including challenges in scalability, material-specific effectiveness, and safety concerns associated with microwave use. Despite these challenges, the microwave-assisted wet precipitation method continues to be a promising approach for β-TCP synthesis, offering significant benefits regarding reaction speed, product quality, and energy efficiency. Ongoing research aims to address its limitations and expand its applications in biomaterials production, making it an increasingly valuable tool in advanced materials synthesis [69].

V. Solid-state reaction method

The solid-state reaction method is a common way to make β-tricalcium phosphate (β-TCP) particles. It involves heating mixtures of calcium and phosphate precursors until they are physically uniform. This method is known for its simplicity, scalability, and ability to produce a diverse range of β-TCP particles with varying properties[46,71]. Common starting materials like calcium carbonate ($CaCO_3$) and DCP, mixed and ground to ensure uniform distribution, typically initiate the process. The mixture is then calcinated at around 1000 °C for several hours, initiating the chemical reaction and promoting the formation of β-TCP. Post-calcination, the material is ground into a fine powder and sieved to achieve the desired particle size distribution, with an

optional sintering step to increase density and particle size [60,71]. While the method offers simplicity, cost-effectiveness, and suitability for large-scale production, it also presents challenges such as high energy consumption, difficulty in achieving single-phase β-TCP, and irregular particle morphology. Recent developments have focused on multi-stage synthesis to produce high-purity β-TCP, thermodynamic modelling to optimize synthesis conditions, and pressure application to improve the quality of the end product. Even with these problems, the solid-state reaction method is still a good way to make β-TCP, especially when purity is not very important or when treatments after synthesis can improve the material's properties.

2.1.3. Dicalcium Phosphate

DCP cements are a class of calcium phosphate materials with a calcium-to-phosphorus (Ca/P) ratio of 1.0 [11,72,73], primarily existing as monetite (DCPA, $CaHPO_4$) and brushite (DCPD, $CaHPO_4 \cdot 2H_2O$). These biocompatible and osteoconductive materials have gained significant attention in biomedical applications, particularly in dentistry and orthopedics [14,23,74,75]. A notable property of DCP cements is that DCPD transforms into DCPA when exposed to temperatures above approximately 80°C, influencing both material processing and in vivo behaviour. DCP cements find diverse applications in bone tissue engineering, dentistry, orthopedics, drug delivery, implant coatings, cancer therapy, and biosensors. Their advantages include excellent biocompatibility, osteoconductivity, bioresorbability, and injectability. However, they face limitations such as extended setting times and poor compressive strength compared to other bone cement types. Recent developments focus on addressing these challenges through composite formulations, ion substitution, and exploration of 3D printing techniques. Despite their limitations, DCP cements' versatility and biocompatibility make them promising materials for various biomedical applications, with ongoing research aimed at expanding their potential uses in tissue engineering and regenerative medicine [23,74,76].

2.1.3.1. Dicalcium Phosphate Dihydrate (Brushite)

DCPD (brushite), commonly known as brushite, is a calcium phosphate biomaterial extensively used in various biomedical applications due to its favourable properties [77]. Brushite can be synthesized into hydraulic cements and is employed in the management of dental and periodontal ailments, augmentation of maxillofacial bones, drug delivery systems, bone reconstruction surgeries, and the treatment of cranial deformities [23,43,78–81]. Brushite crystallizes in the monoclinic crystal system with a space group of Ia, characterized by unit cell parameters: a = 5.8119 Å, b = 15.1867 Å, c = 6.2416 Å, β = 116.405°, and a density of 2.33 g/cm³. One of the notable transformations of brushite is its conversion to monetite (DCPA, $CaHPO_4$) when heated above 80°C, a process that involves the release of water molecules [82–84]. Despite its widespread use, brushite's in vivo performance presents challenges. Brushite can be reabsorbed initially, but it interacts with the body's environment, creating insoluble hydroxyapatite. This makes the resorption rate much slower. This limitation restricts its long-term clinical applications [23,77,81]. Extensive research has been conducted to understand the thermal degradation of DCPD, revealing complex intermediary phases during dehydration that can lead to the formation of crystalline calcium pyrophosphate ($Ca_2P_2O_7$, CPP) [23,73,85]. However, the exact dehydration mechanism remains unclear [73]. Brushite's high solubility under physiological conditions makes it a suitable candidate for rapid resorption and bone regeneration. Formulations often utilize brushite for its quick degradation, particularly in drug delivery systems where it serves as a carrier for therapeutic agents. Additionally, brushite-based materials exhibit excellent bioactivity and biocompatibility, promoting new bone formation without significant inflammatory responses. Recent advancements have focused on enhancing brushite's properties through ionic substitutions, which can modify its structural and morphological features and optimize synthesis conditions to control crystal growth and improve mechanical properties. While brushite has significant advantages in terms of bioactivity and resorption, its tendency to convert to hydroxyapatite in vivo and relatively low mechanical strength pose challenges for long-term applications. Ongoing research aims to address these issues by exploring new synthesis methods, material modifications, and composite formulations to enhance brushite's performance in clinical settings [23,77,81].

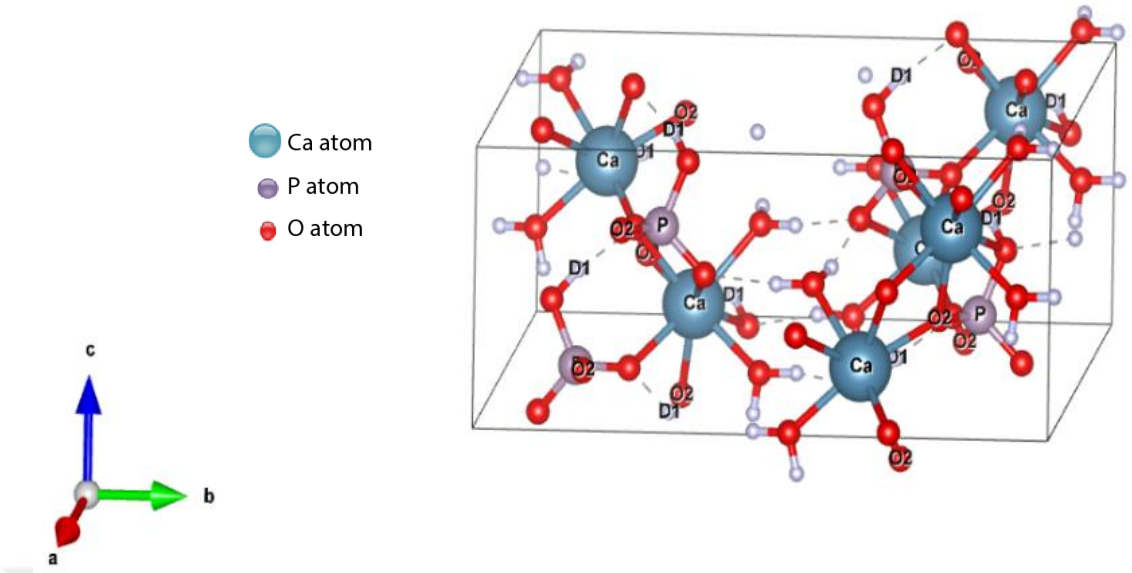

Figure 2.2. Structure of DCPD.

2.1.3.2. Dicalcium Phosphate Anhydrous (Monetite)

Monetite, the common name for DCPA with the chemical formula $CaHPO_4$, is a crucial calcium phosphate compound extensively used in biomedical fields due to its biocompatibility and osteoconductivity [23] It exhibits excellent stability under slightly acidic conditions but dissolves readily in alkaline aqueous solutions [86,87], making it suitable for drug delivery systems, dental procedures, orthopedic treatments, and cranial bone augmentation [43,88–90]. Monetite shares similar chemical composition and solubility characteristics with brushite [23,91] its anhydrous nature provides distinct advantages, such as resistance to reprecipitation into apatite in vivo, allowing for enhanced degradation potential in bone regeneration applications [25,92,93]. Crystallizing in the triclinic crystal system with a P1 space group, monetite has unit cell parameters of a=6.910 Å, b=6.627 Å, c=6.998 Å, α=96.34º, β=103.82º, and γ=88.33º, and a density of 2.93 g/cm³ [83,84,87]. Its solubility decreases with increasing temperature, and its slower crystal growth rate compared to brushite can be advantageous in controlling the setting time and properties of calcium phosphate cements [84]. Monetite has demonstrated significant efficacy in promoting new bone formation, making it a valuable material for bone regeneration [92]. Additionally, its controlled solubility makes it an excellent carrier for therapeutic agents in drug

delivery systems. In dental applications, monetite is used in cements and toothpaste formulations, and in orthopedics, it serves as a coating material for metallic implants to enhance osseointegration. Recent research has focused on enhancing monetite's properties through composite materials, 3D printing for custom bone scaffolds, and ion substitution to improve its osteogenic potential. Overall, monetite offers unique advantages in biomedical applications, with ongoing research to optimize its properties and expand its use in regenerative medicine and tissue engineering.

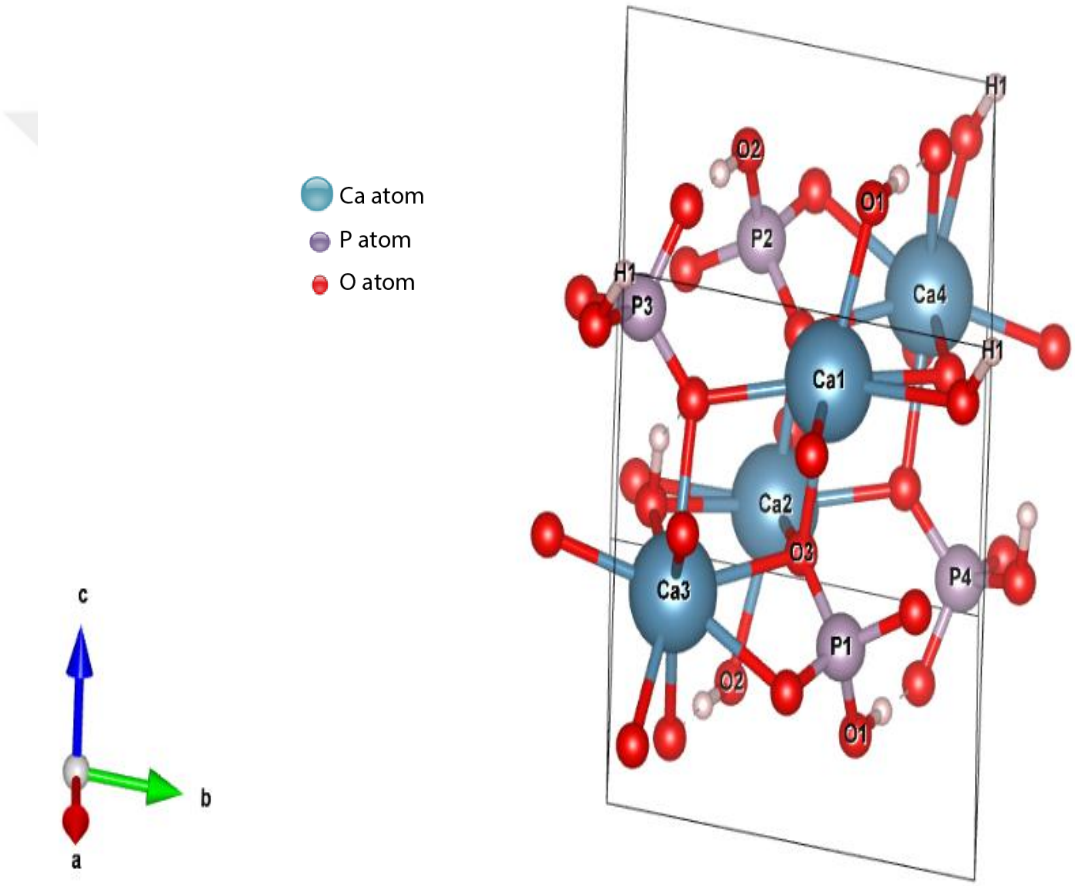

Figure 2.3. Structure of DCPA.

2.2. DICALCIUM SILICATE

C_2S is an important Portland cement component and significantly functions in the calcium-silicate system. Moreover, it demonstrates encouraging prospects in bone

defect regeneration [94]. This is a unique bioactive inorganic compound composed of silicon, calcium, and oxygen, with the addition of $CaO\text{-}SiO_2$ components. The liberation of silicon ions from the C_2S layer plays a crucial role in the mechanism of skeletal growth and regeneration [95]. C_2S is present in five different polymorphic forms, specifically α, α′H, α′L, β, and γ. Out of these several forms, the γ phase is the most stable at ambient temperature, according to thermodynamics.

On the other hand, the β phase is the most reactive among the other forms [96]. Multiple investigations have demonstrated that using Ca_2SiO_4 particle ceramics and coatings has bioactive properties. This leads to the quick production of a bone-like apatite layer on their surface when immersed in simulated bodily fluid (SBF) [97]. The chemical compound C_2S has hydraulic properties and can react with water or an aqueous solution to make calcium silicate hydrate (C-S-H). This process plays a role in the innate ability of a material to establish itself and then naturally improve its strength. The C_2S paste can potentially be administered directly at the location of the defect by injection, eliminating the requirement for massive surgical incisions [98].

Moreover, a prior investigation has shown that Ca_2SiO_4 ceramics possess biocompatibility and can promote the attachment and dissemination of mesenchymal stem cells [99]. Despite the favourable characteristics of C_2S-based biocements, they are unsuitable for clinical applications due to their excessively prolonged self-setting time and poor compressive strength in the early stages [100]. To enhance performance, the setting time of C_2S was reduced by incorporating calcium sulphate hemihydrate, a substance known for rapidly solidifying upon contact with water [101].

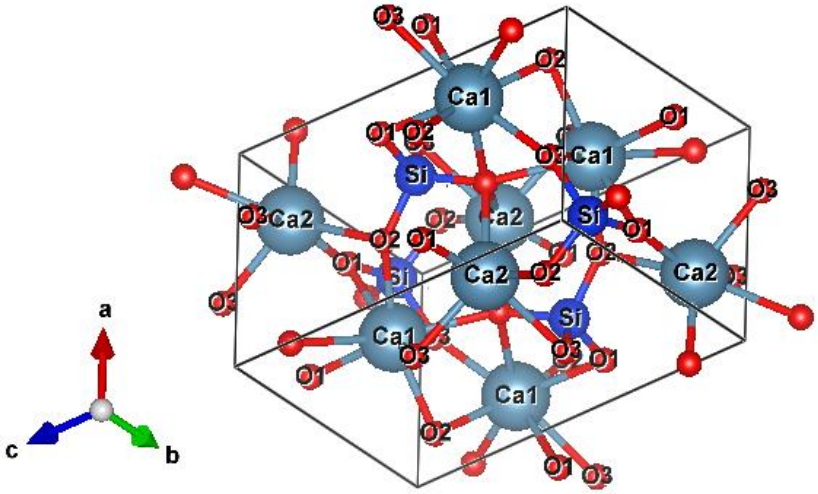

Figure 2.4. The unit cell structure of Ca2SiO4.

CHAPTER 3

MATERIALS AND METHODOLOGIES

3.1. MATERIALS AND CHEMICALS

Calcium nitrate tetrahydrate ($Ca(NO_3)_2 \cdot 4H_2O$), diammonium hydrogen phosphate ($(NH_4)_2HPO_4$), and tetraethyl orthosilicate (TEOS, $Si(OC_2H_5)_4$) were used as sources of Ca^{2+}, PO_4^{3-}, and SiO_2, respectively, to prepare β-TCP/β-C_2S composite materials. Monocalcium phosphate monohydrate (MCPM, $Ca(H_2PO_4)_2 \cdot H_2O$) was used as a precursor to prepare dicalcium phosphate (DCP) cements. Ammonium hydroxide (NH_4OH) was used in this study to adjust the pH value. All materials were purchased from Merck, Germany.

3.2. SAMPLES PREPARATION

3.2.1. Synthesis of β-tricalcium Phosphate Powder

The β-TCP material was produced by microwave-assisted wet precipitation [95]. To prepare Solution (A), For Solution (A), 42.51 grams of $Ca(NO_3)_2 \cdot 4H_2O$ were dissolved in 200 mL of distilled H_2O. Solution (B) was prepared by dissolving 15.85 g $(NH_4)_2HPO_4$ in 200 mL of distilled H_2O. Solution (B) was progressively added to Solution (A) while stirring. NH_4OH was added to adjust the solution's pH to 7. After 30 minutes of stirring at room temperature, the mixture was microwaved for 5 minutes at 800 watts in a SAMSUNG MS23F301EAW microwave oven. The product was then filtered and rinsed with distilled H_2O. The sample was dried overnight at 80°C in an oven. Finally, the resulting white powder was heat-treated at 1000°C for 2 hrs.

3.2.2. Synthesis of β-Dicalcium Silicate Powder

β-C_2S was synthesized using the sol-gel technique. A calcium-to-silicon (Ca/Si) molar ratio of 1.4:1 was employed. The synthesis began by dissolving TEOS in a mixture of ethanol and distilled water (1:2:4 volumetric ratio of TEOS:water: ethanol). After 30 minutes of agitation, 0.5 mL of acetic acid solution was added as a catalyst to initiate TEOS hydrolysis. The solution was stirred at ambient temperature to ensure complete hydrolysis, adding 0.5 moles of $Ca(NO_3)_2 \cdot 4H_2O$. This mixture was stirred at 60°C for 6 hours, then left at room temperature for 24 hours to allow gelation. The resulting hydrogel was dehydrated at 80°C for 48 hours, followed by calcination at 800°C (10°C/min heating rate) for 3 hours [102].

3.2.3. Synthesis of β-Dicalcium Silicate / Dicalcium Phosphate Cement Composites

The pure phase of DCP cement was prepared by mixing 1.0 g of β-TCP and 0.5 g of MCPM powders in a mortar. Precisely 0.8 mL of distilled H_2O was added to the powder mixture and vigorously mixed until a homogenous paste was achieved, which subsequently self-hardened at room temperature. The β-C_2S/DCP cement composites were prepared using a similar protocol. Various amounts of β-C_2S powder were combined with β-TCP and MCPM powders. The mixture was thoroughly blended, and a suitable amount of water was added at a ratio of 0.8 mL per 1.5 gram of powder. Different β-C_2S/DCP cement composites were prepared, as summarized in Table 3.1.

Table 3.1. Various compositions of pure DCP and β-C_2S/DCP cement composites

Sample ID	**Solid Phase**			**Liquid Phase**
	β-TCP (g)	**MCPM (g)**	**β-C_2S (g)**	**H_2O (ml)**
Pure phase (DCP)	1.00	0.50	0.00	0.80
20 % β-C_2S/DCP	1.00	0.50	0.30	0.95

30 % β-C_2S/DCP	1.00	0.50	0.45	1.025
40 % β-C_2S/DCP	1.00	0.50	0.60	1.10

3.3. MICROSTRUCTURAL CHARACTERIZATIONS

The researchers utilized several approaches to analyze the properties of the manufactured cements. XRD was employed to determine the cements' phases and measure their lattice characteristics. Additionally, the SEM method was utilized to examine the morphology and dimensions of the particles. The existence of functional groups was confirmed using the technique of FTIR. At the same time, the thermal stability of the materials was studied using TGA done under a nitrogen atmosphere, with temperatures ranging from ambient to 950°C.

3.3.1. X-Ray Diffraction:

XRD (Figure 3.1) analysis was conducted to characterize the crystalline phases, determine lattice parameters, and assess the purity of the prepared cement materials. The experiments were performed using a Rigaku Ultima IV multipurpose X-ray diffractometer, representing the state-of-the-art XRD systems. The XRD measurements were conducted at room temperature, scanning over a 2θ range from 10° to 90°. A step size of 0.02° was employed, within the recommended range of ≤0.05° for high-quality diffraction data. The scanning speed was set to approximately one minute per step to ensure sufficient intensity and resolution of the diffraction peaks. This relatively slow scanning speed allows for better peak shape definition and improved signal-to-noise ratio, crucial for accurate phase identification and quantification.

The diffractometer was operated using CuKα radiation, with the X-ray tube typically set at a voltage of 40 kV and a current of 40 mA, as these are common settings for cement analysis.

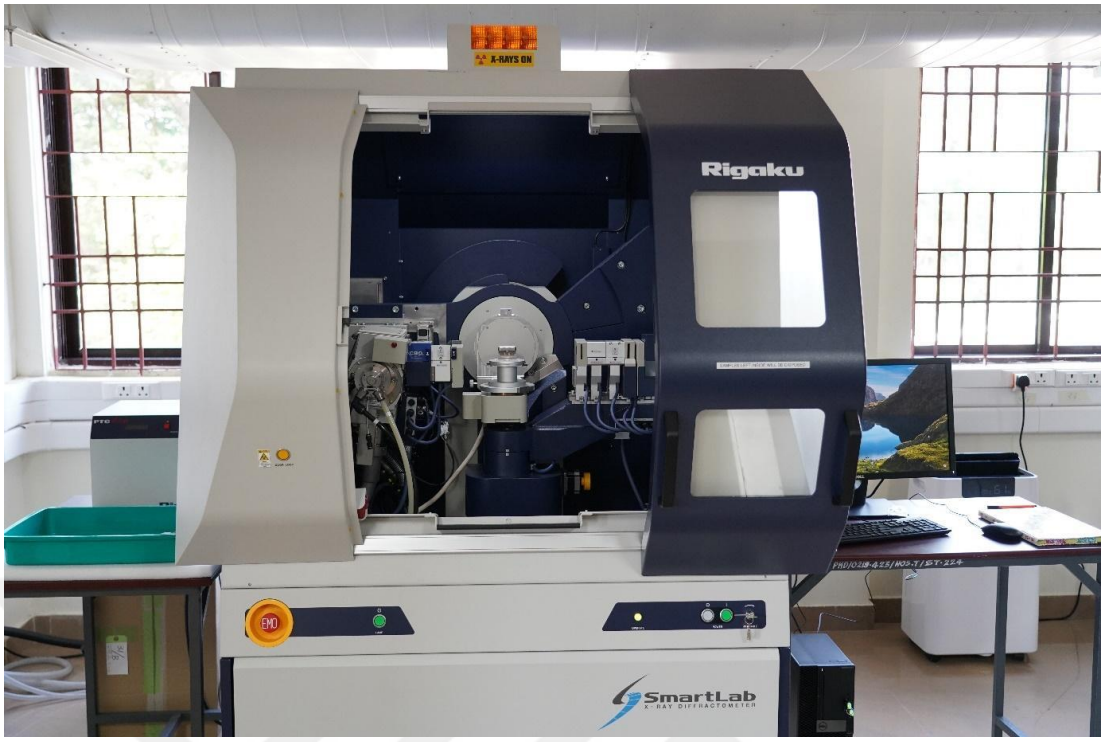

Figure 3.1. XRD device.

3.3.2. Fourier-Transform Infrared Spectroscopy

The functional groups in the cement samples were characterized using FTIR (Figure 3.2), employing a Bruker VERTEX 70v spectrometer. This advanced analytical technique provides valuable insights into cementitious materials' molecular structure and composition. The FTIR analysis was conducted in transmission mode, particularly suitable for studying powdered samples like cement.

The spectra were acquired over a comprehensive wavenumber range from 4000 to 400 cm^{-1}, encompassing the mid-infrared region. This range is crucial for identifying key functional groups and molecular bonds of cement compounds.

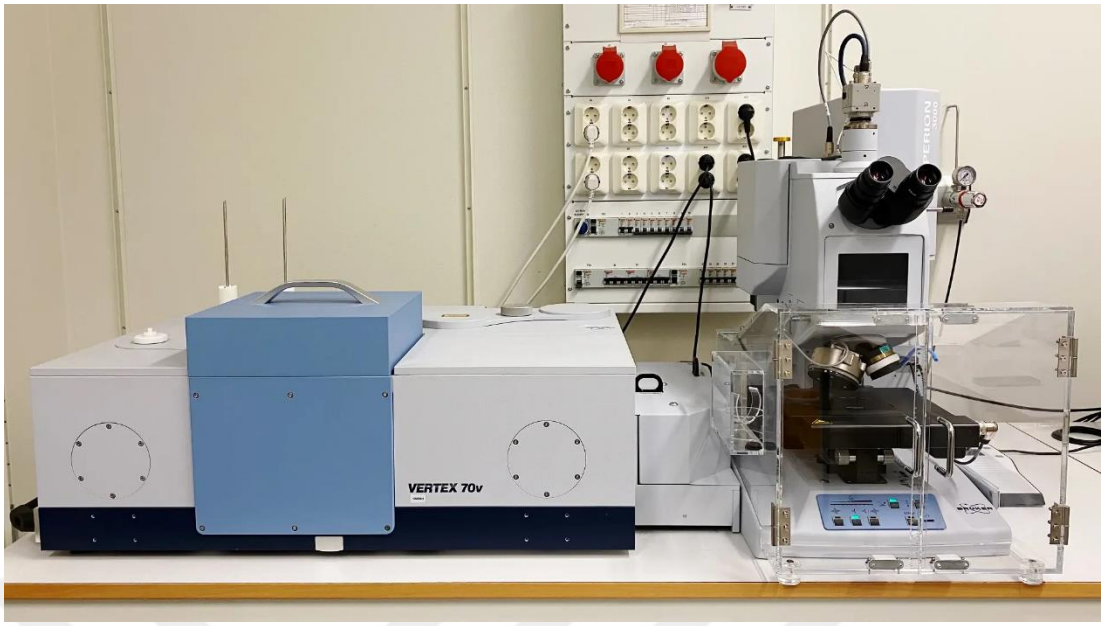

Figure 3.2. FTIR device.

3.3.3. Scanning Electron Microscopy

A Carl Zeiss Ultra Plus Gemini SEM (Figure 3. 3) analyzed particle size and morphology. This high-resolution field emission SEM (FE-SEM) is equipped with advanced detectors, including the In-lens and SE-Detector for high-resolution imaging. To minimize charging effects, which can distort the images of non-conductive samples, the cement particles were pre-coated with a thin film of gold using a sputter coater. This process involves depositing a nanometer-thick layer of gold onto the sample surface under vacuum conditions, which improves electrical conductivity and image quality. The SEM analysis provided detailed images of the particle morphology and size distribution.

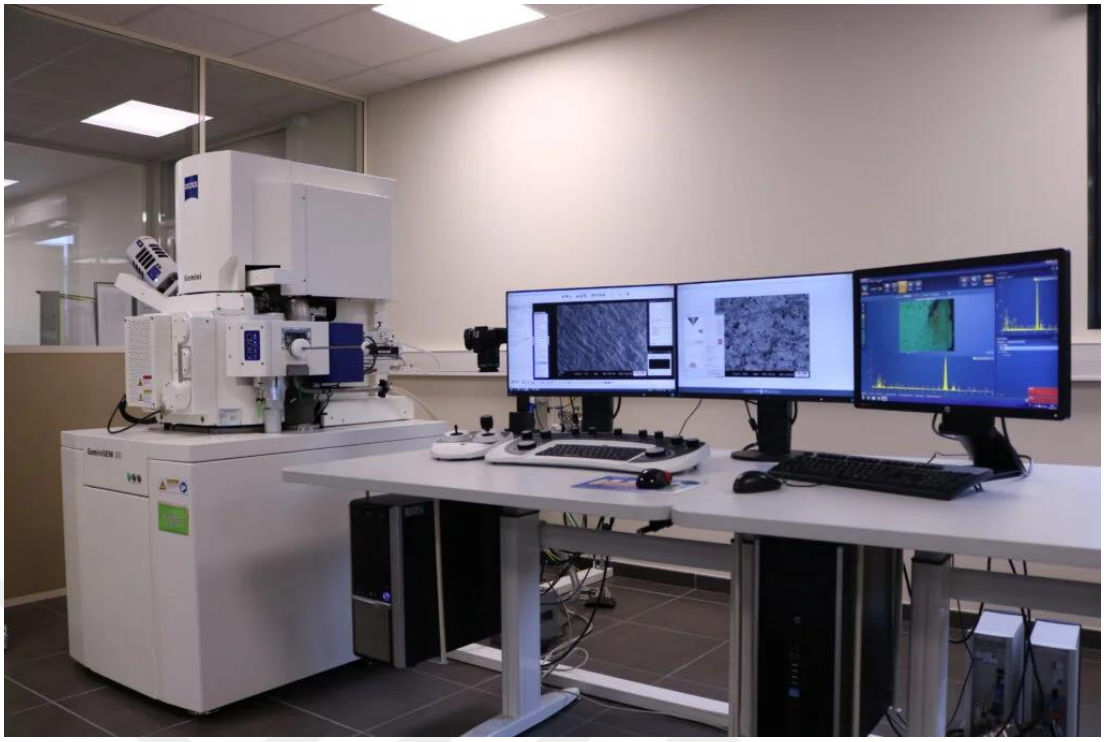

Figure 3.3. SEM device.

3.3.4. Thermogravimetric Analysis

TGA (Figure 3. 4) was performed using a PerkinElmer STA 6000 simultaneous thermal analyzer to evaluate the thermal stability and composition of the prepared cement materials. The STA 6000 combines the capabilities of TGA with differential thermal analysis (DTA) or differential scanning calorimetry (DSC), allowing for simultaneous measurement of weight changes and heat flow.

The analysis was conducted under a controlled nitrogen atmosphere to prevent unwanted oxidation reactions. Samples weighing approximately 10-20 mg were heated over a temperature range of 30°C to 950°C, with a heating rate of 10°C per minute. This temperature range is suitable for observing various decomposition reactions in cement materials, including the dehydration of calcium silicate hydrates.

Figure 3.4. Thermogravimetric analyzer.

3.4. COMPRESSIVE STRENGTH TEST

Adding all admixtures to dental cement may result in a deterioration of its mechanical qualities. The formation of pores can lead to this adverse impact. The comprehensive blending of particles in the base material significantly impacts the uniform dispersion, hence influencing the physical characteristics of cement. Porosity can occur due to the introduction of significant quantities of air during the mixing process. These holes, together with the pores, result from the evaporation of specific quantities of the monomer inside the larger mass [103,104].

The cement samples were cast in cylindrical scaffold shapes (6 mm in diameter and 12 mm in height). Compressive properties were analyzed at room temperature using a Universal Testing System (Instron 5565 A, USA) according to the standard test method

ASTM F451-16. The experiments were conducted in triplicate at a compression velocity of 4 mm/min.

3.5. IN VITRO ANTIBACTERIAL ACTIVITY

The Gentamicin sulphate (Merck-Germany) compound was dissolved in distilled water at a concentration of 2 mg/mL. Subsequently, the resulting aqueous solution was combined with the powder to formulate the cement. The broth microdilution method was used to determine the antimicrobial activity of the samples [105]. Sample extracts were prepared by following ISO 10993 standards for biomaterial testing with a recommended concentration of 0.2 g/mL in sterilized LB broth media. The extracts were incubated for 24 h, at 37°C then sterilized by a 0.22 μm pore-sized filter. The serial dilutions (0.2 g/mL, 0.1 g/mL, 0.05 g/mL, 0.025 g/mL, 0.0125 g/mL, 0.00625 g/mL) were prepared from the extract with an initial 0.2 g/ml concentration in 96 well plates. Staphylococcus aureus (S. aureus, gram-positive, ATCC 6538) was cultured overnight at 37°C following the aseptic technique requirements. For the optical density (OD) control, the overnight culture of S. aureus was sub-cultured, and the OD600 values were measured hourly. 10 μl of S. aureus samples (OD600=0.4) were inoculated in 96 well plates with the extracts. The OD600 measurements were repeated in 0 h and 24 h with the microplate reader.

3.6. IN VITRO CELL CULTURE STUDIES

3.6.1. Cell Culture Preparation

The Gentamicin antibiotic was solubilized in distilled water at a concentration of 2 mg/ml. Subsequently, the resulting aqueous solution was combined with the powder to formulate the cement groups. The Osteosarcoma (Saos-2) cell line was cultured in Dulbecco's MEM (DMEM; Merk Germany) containing 10% heat-inactivated fetal bovine serum (FBS) and 1% penicillin/streptomycin (Invitrogen, USA) at 37 °C in a 5% CO_2-containing environment.

3.6.2. Cell viability assay

The effect of target samples on the viability of Saos-2 cells was determined using the Deep Blue assay. The compressed and disc-formed versions of the samples were UV sterilized, and discs were placed in a 24 well plate containing DMEM and incubated for 24 h. After the incubation, the media was discarded, and 1×104 Saos-2 cells were seeded in a 20 µL drop-on disc sample. After 2 h for the cells to attach to the discs, the medium was completed to 100 µL, and the plate was incubated at 37 °C. For the Deep Blue assay, Deep Blue reagent was added to each well to obtain a 10% final concentration, and the plate was incubated for 4h. After incubation, the Deep Blue reagent containing media was transferred into the new 24-well plate for fluorescence measurement. Since the deep blue reagent does not harm the cells, after removing the deep blue reagent-containing media, Saos-2 cells continued to grow with adding the fresh medium. A microplate reader (Varioskan Flash Spectral Scanning Multimode Reader, Thermo Scientific) was used for the 530–590 nm fluorescence measurement. The measurements were repeated on day 1, day 4, and day 7.

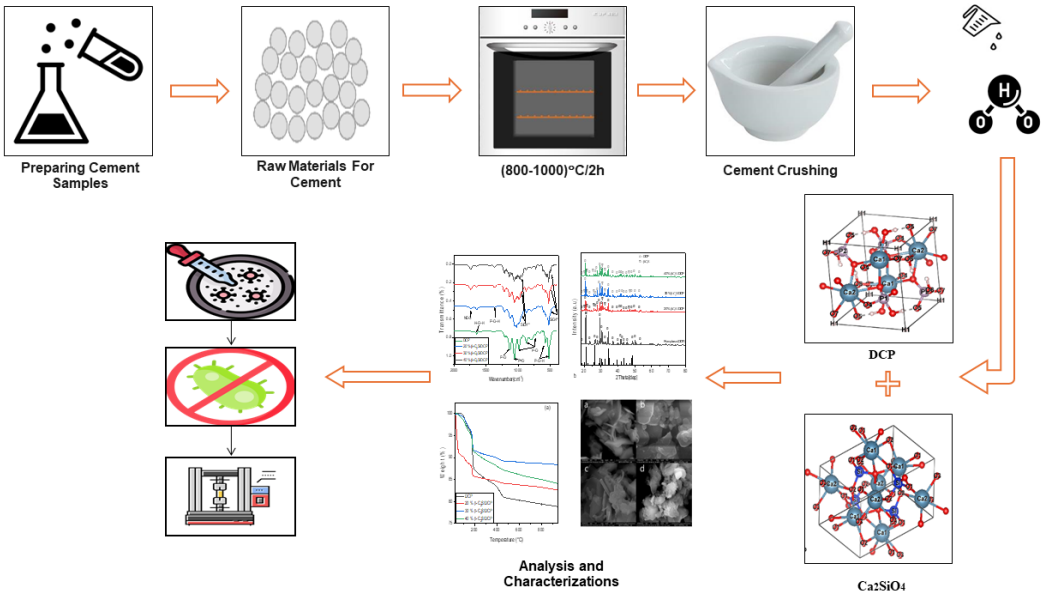

Figure 3.5. Experiment flow chart.

CHAPTER 4

RESULTS AND DISCUSSION

4.1. STRUCTURAL CHARACTERIZATION OF β-TCP

Figure 4.1. illustrates the diffraction pattern seen in β-TCP powder. The diffraction peaks seen in the man-made β-TCP were very similar to those seen in the standard β-TCP phase (whitlockite phase, JCPDS 09–0169). The analysis detected no additional calcium phosphate (CP) phases. In particular, the analysis showed no clear peak at 32.196°. This meant that the powder that was made was uniform and did not contain the hydroxyapatite phase (JCPDS 09–432). The consistency of these findings with those of other studies provides further evidence for the reliability and repeatability of the synthesis methods used to produce β-TCP.

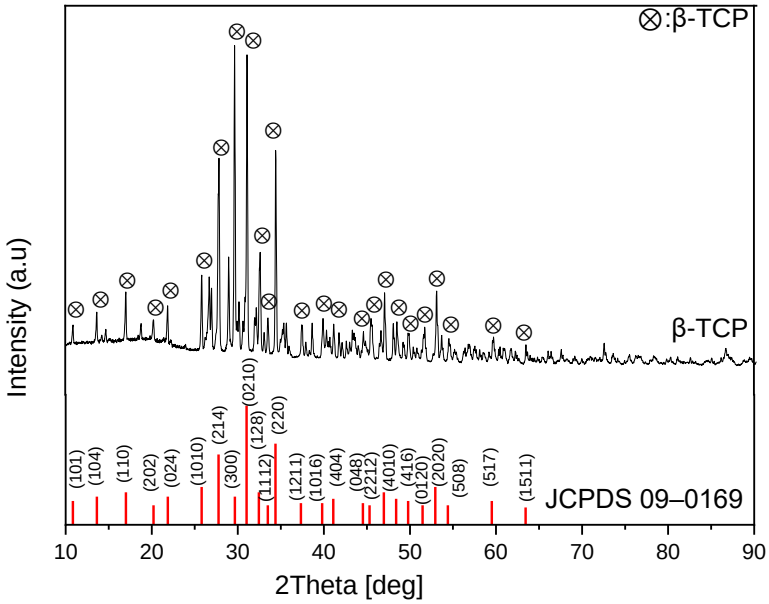

Figure 4.1. XRD pattern of β-TCP calcined at 1000 ºC for 2 h.

Figure 4.2. displays SEM images of β-TCP powder. The β-TCP particles had a spherical morphology with smooth contours, and they fused because they were subjected to high-temperature heat treatment. Nevertheless, prior research has also revealed comparable findings [106–108]. Grigoraviciute-Puroniene et al. The researchers produced TCP particles using the microwave-assisted approach and calcined them at 1000 °C for 2 hours. The researchers noted that the average size of the particles obtained in their study was approximately 150 nm [106]. Previous research reported a size smaller than this one. This difference can be attributed to the rapid growth of particles during the heat treatment process. The Ca/P ratio was also determined to be 1.39, slightly lower than the desired value of 1.5.

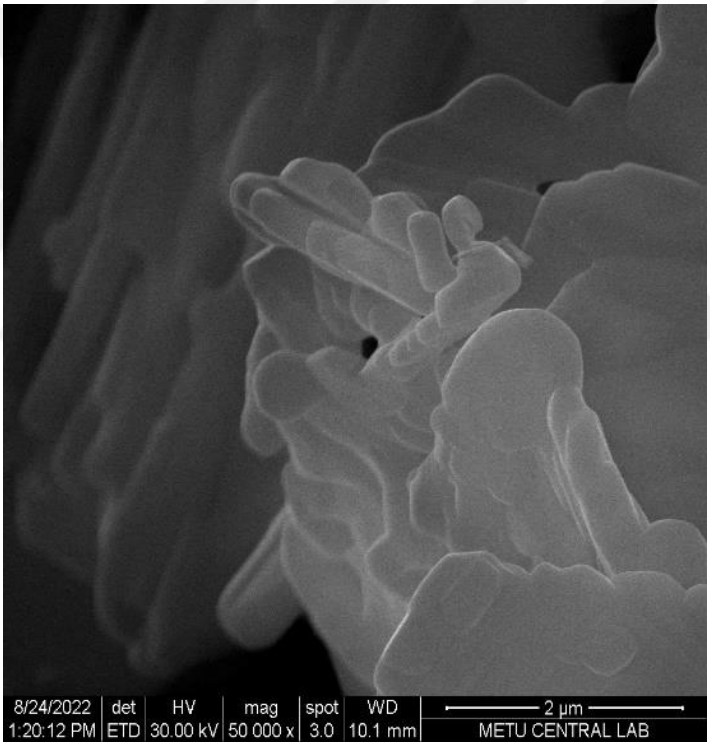

Figure 4.2 SEM image of β-TCP sample calcined at 1000 ºC for 2 h. Scale bar is 2µm.

Figure 4.3 presents the FTIR spectra of the -TCP powders. Table 4.1 details the characteristic peaks of β-TCP observed in the FTIR spectrum. The band observed at 551.07 cm^{-1} is attributed to the vibrational mode of PO_4^{3-} (υ4) [20,109]. The positions and forms of the peaks closely corresponded to the FTIR results of the prior research. The peak at 724 cm^{-1} indicated the presence of $P_2O_7^{4-}$ ions, which are part of the β-TCP precursor β-calcium pyrophosphate. This peak's increased sharpness confirms the

transformation of HPO_4^{2-} into β-TCP through calcination at 1000°C. The bands within the range of 937.97 cm^{-1} to 1214.32 cm^{-1} were identified as the ν_1 (symmetric stretching) and υ_3 (asymmetric stretching) modes of the PO_4^{3-} group. These peak positions and forms closely matched the FTIR data from prior research [20,110]. The bands at 1022.72 and 1066.93 cm^{-1} are attributed to the stretching vibration characteristic of υ3 [111]. The peak at 1144.31 cm^{-1} is likely attributed to the triply degenerate υ3 antisymmetric P–O stretching modes [112]. The signal at 1365.4 cm^{-1} is ascribed to residual nitrate groups from synthesized precursors [113]. The absorption band at 1733 cm^{-1} is associated with the characteristic peak of the C=O bond [114]. The absence of stretching and bending bands at 3001 cm^{-1} confirms the successful synthesis of single-phase β-TCP, as these bands correspond to the hydroxyl (-OH) group [20].

Table 4.1. Characteristic peaks of β-TCP in the FTIR spectrum.

Peak number	Wavelength (cm^{-1})	Band assignment
1	551.07	$PO4^{-3}$ vibrational mode of (υ4)
2	724	$P_2O_7^{-4}$ ions
3	937.97	$PO4^{-3}$ symmetric stretching mode of (υ1)
4	1022.72	$PO4^{-3}$ asymmetric stretching mode of (υ3)
5	1066.93	$PO4^{-3}$ asymmetric stretching mode of (υ3)
6	1144.31	$PO4^{-3}$ asymmetric stretching mode of (υ3)
7	1214.32	$PO4^{-3}$ asymmetric stretching mode of (υ3)
8	1365.4	the nitrate ion (NO^{-3})
9	1733	the C=O bond
10	3001	the stretching of the O-H bonds

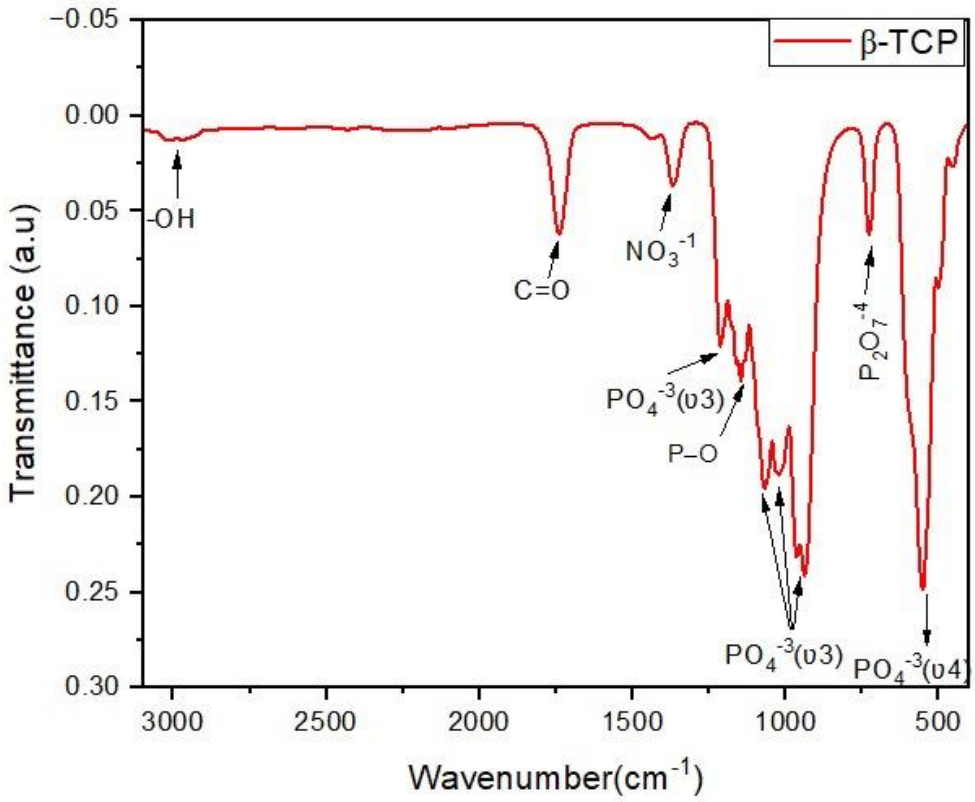

Figure 4.3. FTIR spectrum of β-TCP powder that underwent calcination at a temperature of 1000 °C for 2 hours.

4.2. CHARACTERIZATION OF β-DICALCIUM SILICATE

The XRD patterns of β-Ca_2SiO_4 (β-C_2S) powder that was made using the sol-gel method can be seen in Figure 4.4. The observed patterns correspond to the confirmed diffraction data for β-C_2S (PDF-2 33-0302) [115]. Contaminants like calcium oxide (CaO) and silicon dioxide (SiO_2) were absent from the powders generated [116]. The synthesized C_2S exhibited significant crystallinity, as shown by the sharp and narrow diffraction peaks. The crystallization rate was 82.6%.

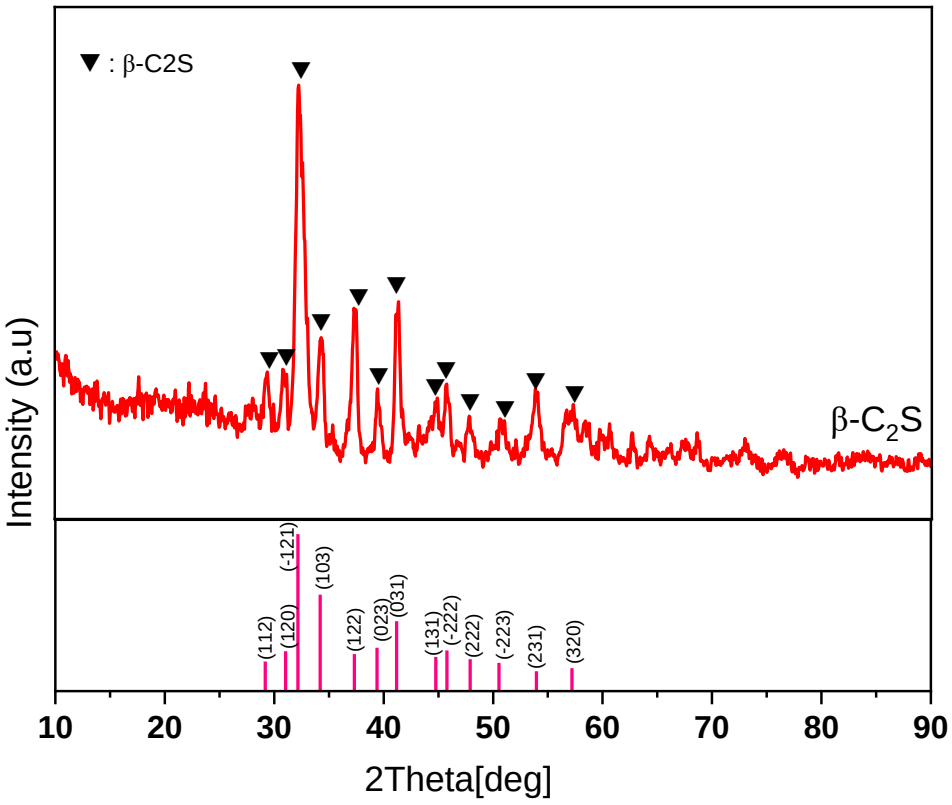

Figure 4.4. XRD patterns of pure β-C_2S powder calcined at 800◦C for 3h.

Figure 4.5 displays the FTIR spectra of β-C_2S powder, while Table 4.1 shows the specific peaks associated with β-C_2S. The silicate clusters have discernible absorption bands. It is important to notice that there are significant peaks at 484 cm^{-1}, which correspond to the asymmetric bending mode Si-O ν_4 (SiO_4^{-4}). Furthermore, the signal detected at 947 cm^{-1} is linked to the asymmetric bending mode Si-O ν3 (SiO_4^{-4}) [117]. Additionally, bands falling within the spectral range of 1216 – 1441 cm^{-1} have been seen, indicating a little presence of carbon dioxide [118]. In addition, a peak at the wavelength of 1740 cm^{-1} indicates that the absorption band is mostly associated with the nitrate ion (NO_3^{-1}) [119]. The band detected at a wavenumber of 3004 cm^{-1} corresponds to the vibrational mode linked to the elongation of the O-H bonds.

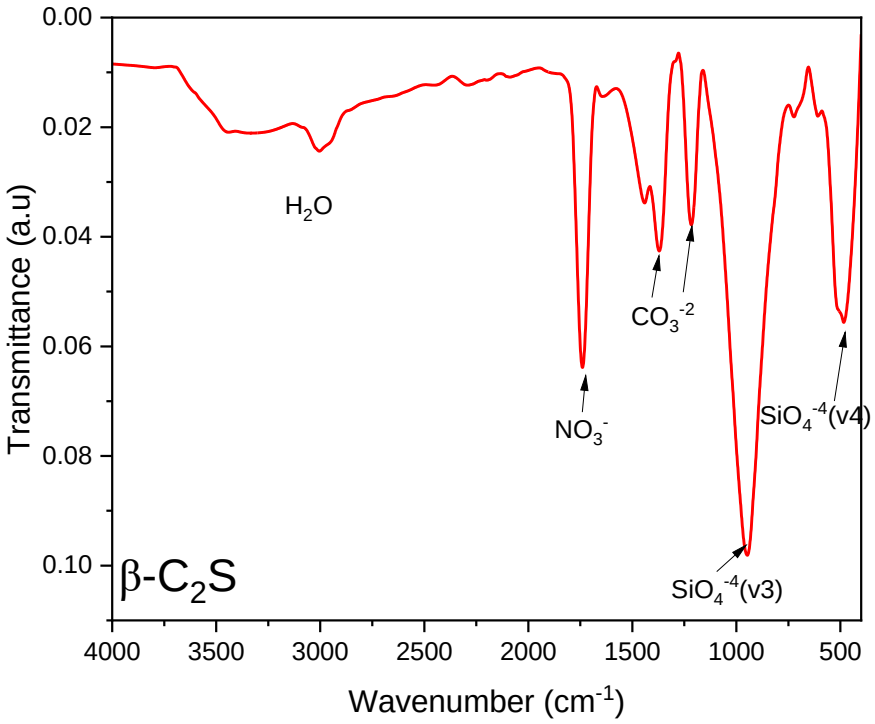

Figure 4.5. FTIR pattern of β-C_2S powder calcined at 800◦C for 3h.

Table 4.2. Characteristic peaks of β-C_2S in the FTIR spectrum.

Peak number	Wavelength (cm^{-1})	Band assignment
1	484	the asymmetric bending mode Si-O ν4 (SiO_4^{-4})
2	947	the asymmetric bending mode Si-O ν3 (SiO_4^{-4})
3	1216	stretching C-O
4	1441	stretching C-O
5	1740	the nitrate ion (NO_3^{-1})
6	3004	the stretching of the O-H bonds

Figure 4.6 shows an SEM picture of β-C_2S powder. It shows a smooth, sticky surface with tiny holes and particles that are connected to each other.

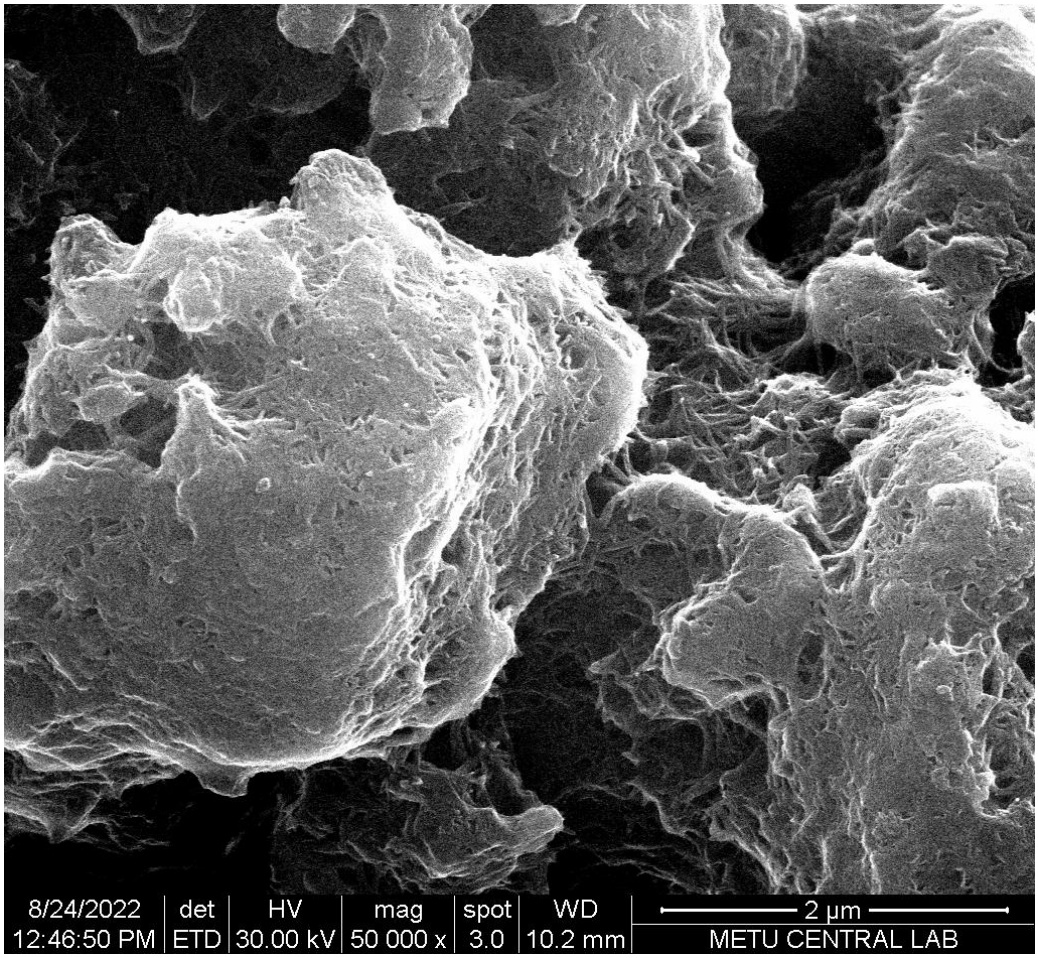

Figure 4.6. SEM image of β-C_2S powder calcined at 800◦C for 3h. Scale bar is 2 µm.

4.3. MICROSTRUCTURE AND BIOLOGICAL PROPERTIES of PURE DCP AND β-C_2S/DCP CEMENT COMPOSITES

Figure 4.7 presents the XRD patterns of pure DCP and DCP/β-C_2S cements set at room temperature. XRD peaks revealed the highest levels of intensity at two values: 20.95°, 29.2°, 30.6°, 34.1°, and 34.3°. The samples mostly consisted of the brushite phase (JCDPS 72–1240) and the monetite phase (JCPDS 71–1760). According to the JCDPS reference patterns, this cement is closer to the brushite phase[20,104,120]. If a peak is not observed at 20.95°, it suggests that the prepared DCP exists in the form of monetite (JCPDS 71-1760) and that the brushite phase (JCPDS 72-1240) is not present [20]. Upon the addition of β-C_2S to DCP cement, alterations in the intensity and morphology of the peaks were apparent. After adding β-C_2S to the cement mixture, a significant decrease in the highest level of intensity was detected at an angle of 2θ =

29.2°. The XRD pattern shows an increase and decrease in the degree of crystallinity inside the particles due to adding different concentrations of β-C_2S. This observation is consistent with previously reported results in the literature [121,122]. Moreover, the study found that β-TCP led to an elevation in retinal parameters (a,c), as shown in Table 4.3. The typical lattice parameters for DCP are "a" with an approximate value of 6.9160, and "c" with an approximate value of 6.9460. However, a slight decrease in the "a" axis suggests a more compact crystal structure, whereas a slight increase in the "c" dimension may be attributed to variations in the probability of replacement between different samples and due to lattice strain. Reduced crystal size may be very advantageous for biological applications; increased crystal size is advantageous for improving mechanical characteristics and frequently leads to a larger surface area. This, in turn, promotes cell adhesion and proliferation, which is crucial in dental implant applications, where integrating the material with the biological tissue is essential for success. The increased interaction between smaller β-C_2S molecules led to an increase in unit cell size. We believe this to be the cause of the observed shift of the diffraction peak towards the lower corners [104,121,122].

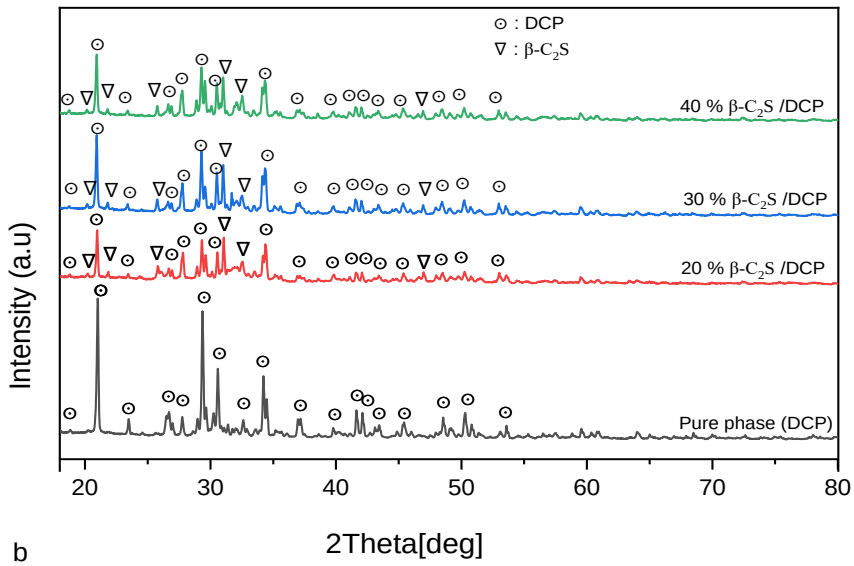

Figure 4.7. XRD patterns of pure DCP and β-C_2S / DCP cement composite.

Table 4.3. Lattice parameters of pure DCP and β-C_2S/DCP cement composites.

Sample ID	Å (A)	C(Å)	CV(Å)^3	Crystallinity (٪)	Crystallite size (nm)
β-TCP	10.4290	37.3800	3520.91	99.390 %	35.07594
DCP	6.9160	6.9460	306.97	93.415 %	36.72502
20 % β-C_2S/DCP	6.9000	7.0000	309.87	98.763 %	23.10064
30 % β-C_2S/DCP	6.9000	7.0000	309.87	95.710 %	26.03445
40 % β-C_2S/DCP	6.9100	6.9980	309.28	99.008 %	29.99831

The FTIR spectrum was employed to analyze the functional groups present in the produced cements. Figure 4.8 presents the results, while Table 4.4 summarizes the characteristic peaks. The peaks exhibited a more confined shape, indicating structural modifications likely induced by the excess presence of β-C_2S. Specifically, the peak observed at 495 cm^{-1} corresponds to the bending vibrations of Si-O-Si chemical bonds [123,124]. This peak shows how silicon and oxygen atoms interact within the structure of the cement. It shows how β-C_2S is added and how it changes the structural properties of the cement, as determined by FTIR analysis. Furthermore, two peaks detected at 522 cm^{-1} and 578 cm^{-1} indicate the stretching mode of the P–O–H bond in HPO_4^{-2}, attributing these vibrations to specific chemical bonds within the cement matrix. Another prominent peak at 871 cm^{-1} is attributed to the bending motion of P–O bonds [125]. The signal at 937 cm^{-1} corresponds to the asymmetric bending mode of Si-O υ3 (SiO_4^{-4}), further characterizing the presence of silicon-oxygen bonds in the cement structure [126]. Between 984 cm^{-1} and 1133 cm^{-1}, a broad band is observed, which is assigned to the stretching vibrations of the P–O bonds [20]. Additionally, the peak at 1058 cm^{-1} is assigned to the stretching mode of P=O, indicating the presence of phosphate groups [74]. The spectral peak around 1211 cm^{-1} suggests a minor presence of carbon dioxide [127]. While the peak at 1367 cm^{-1} corresponds to the bending motion of P–O–H bonds [20]. Moreover, the band at 1647 cm^{-1} is attributed to the bending and stretching vibrations of unbound water molecules (H–O–H bonds), highlighting the presence of hydration within the cement matrix [20,125]. Finally, the peak at 1737 cm^{-1} signifies the absorption band primarily associated with NO^{-3} groups [119].

Table 4.4. Characteristic peaks of cements in the FTIR spectrum.

Peak number	Wavelength (cm^{-1})	Band assignment
1	495	Si-O-Si chemical bonds
2	522	P–O–H stretching mode of the HPO_4^{-2}
3	578	P–O–H stretching mode of the HPO_4^{-2}
4	871	P–O bending mode of the HPO_4^{-2}
5	937	Si-O the asymmetric bending mode of v3 (SiO_4^{-4})
6	984	P–O the stretching mode of the HPO_4^{-2}
7	1058	P=O the stretching mode of of the HPO_4^{-2}
8	1133	P–O the stretching mode of the HPO_4^{-2}
9	1211	the C=O bond
10	1367	P–O–H in-plane bending mode of the HPO_4^{-2}
11	1647	H–O–H bending mode
12	1737	the nitrate ion (NO^{-3})

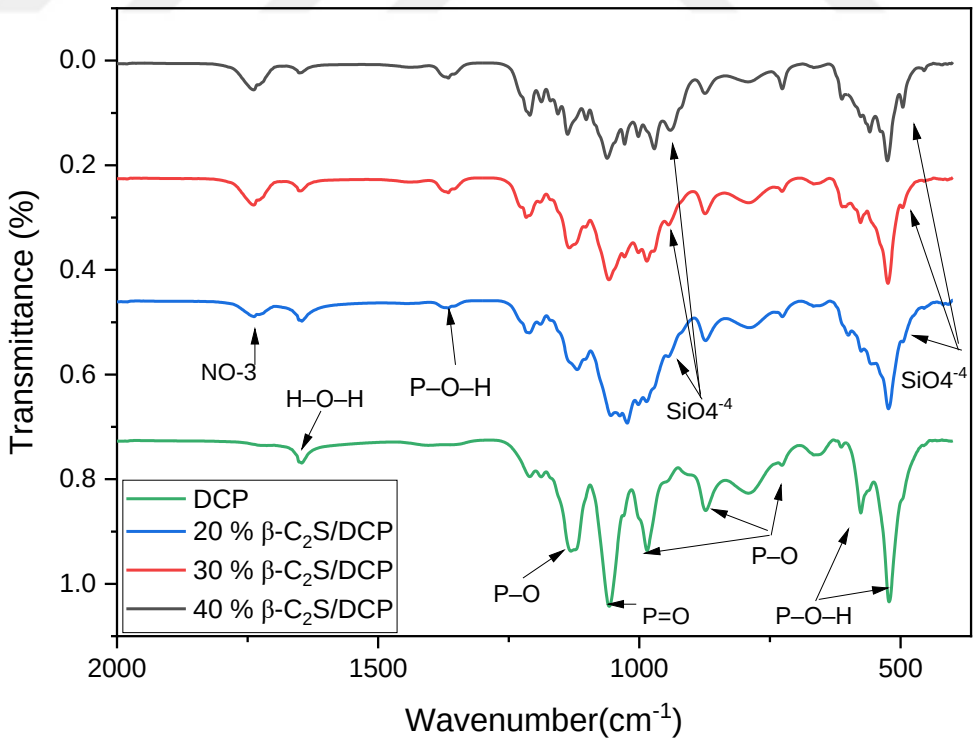

Figure 4.8. FTIR patterns of pure DCP and β-C_2S / DCP cement composites.

Figure 4.9 depicts the microstructure of both pure DCP cement and β-C_2S/DCP composite cement. The SEM analysis revealed distinct characteristics of the particles in each material. Pure DCP particles exhibited a significant, non-symmetrical plate-like structure, with average widths ranging from micro to nanometer dimensions. Variations in plate diameters were attributed to differing agglomeration levels, a phenomenon noted in previous studies [128,129]. In contrast, adding 20% β-C_2S resulted in a highly cross-linked structure. This modification was characterized by the development of a fibrous surface on the cement particles and the presence of minor pore formations. As the proportion of β-C_2S increased to 40%, the microstructure showed a notable shift. Plate-like particles became more prominent and exhibited a slightly spherical shape, indicative of a more homogeneous distribution within the cement matrix [130,131]. These findings show that β-C_2S changes the microstructural properties of the cement and emphasizes its role in changing the shape and distribution of the particles. The SEM analysis provides visual evidence of how varying compositions affect the cement composites' physical properties and structural integrity.

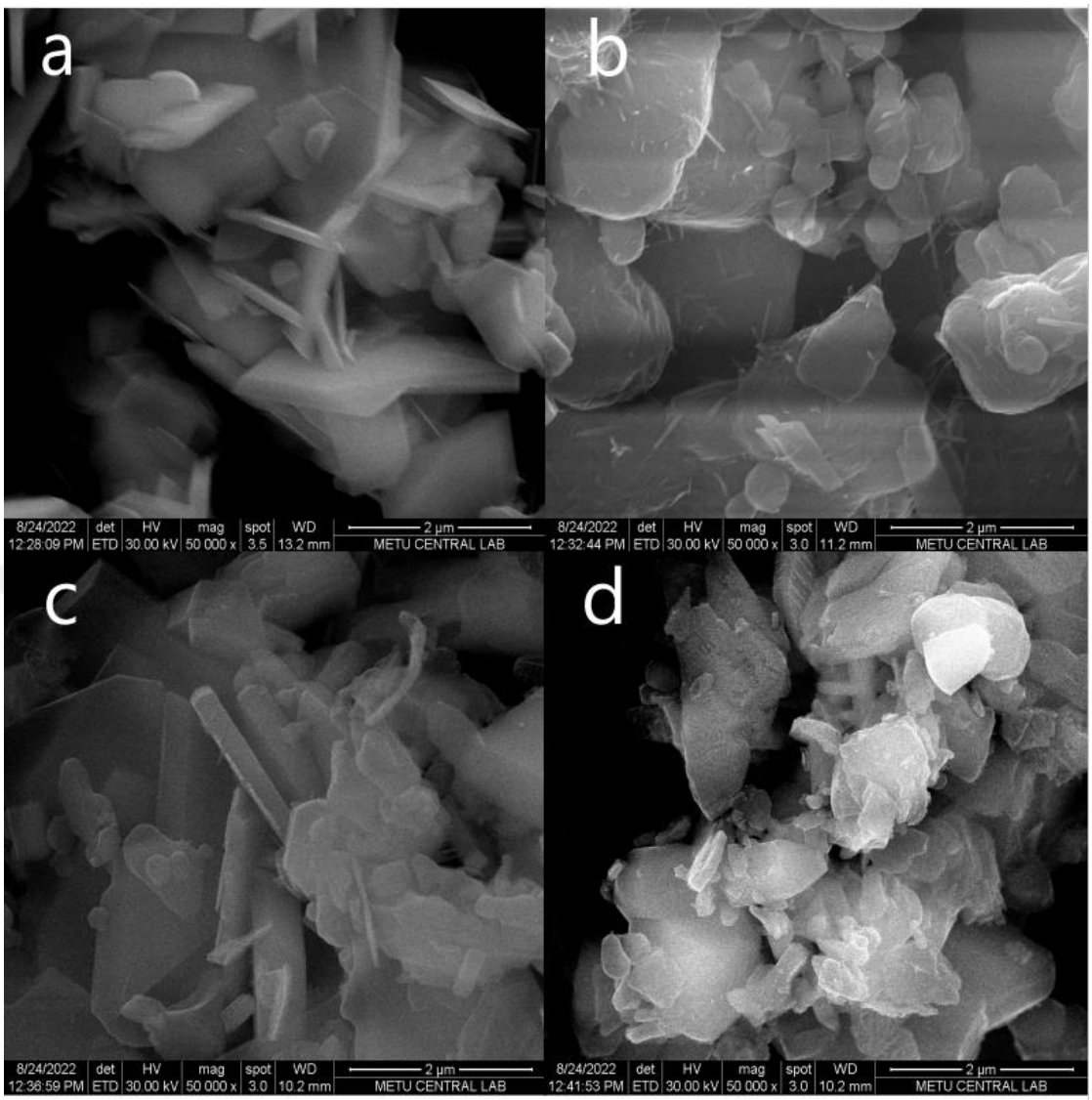

Figure 4.9. SEM images of (a) pure DCP cement (b) 20% β-C_2S/ DCP, (c) 30% β-C_2S/ DCP and (d) 40% β-C_2S/ DCP cement. Scale bar is 2µm.

Figure 4.10 illustrates the thermal analysis results, specifically the TGA/DTA data for the cement samples formulated according to the specifications in Table 3.1. The analysis reveals three distinct stages of weight loss in pure DCP cement occurring within temperature ranges of 50–190 °C, 190–480 °C, and 480–700 °C. The initial stage, occurring from 50 to 190 °C, primarily involves the removal of residual moisture and chemically bound water [20,132]. In the subsequent stage, between 190 and 480 °C, the decomposition of nitrate compounds used in the formulation results in a chemical reaction where two molecules of $CaHPO_4$ break down, eliminating water

molecules and forming calcium pyrophosphate ($Ca_2P_2O_7$), as described by the equation [20,133,134].:

$$2CaHPO_4 \longrightarrow Ca_2P_2O_7 + H_2O \quad \textbf{Eq. 1}$$

The third stage, occurring between 480 and 700°C, involves the decomposition of organic substances and the degradation of $Ca(OH)_2$. Above 700°C, there is negligible further weight reduction, a finding consistent with observations at 800°C, indicating that the samples stabilize after calcination beyond this temperature threshold, in line with prior research [20,135]. Incorporating β-C_2S into the cement mixture resulted in a lower rate of weight loss. Additionally, all samples exhibited thermal stability at temperatures of 700°C and higher. Notably, the TGA curve for the 20% β-C_2S/DCP sample displayed elevated humidity levels. The respective weight loss percentages for pure DCP, 20% β-C_2S/DCP, 30% β-C_2S/DCP, and 40% β-C_2S/DCP were 21.205%, 17.368%, 11.576%, and 15.890%.

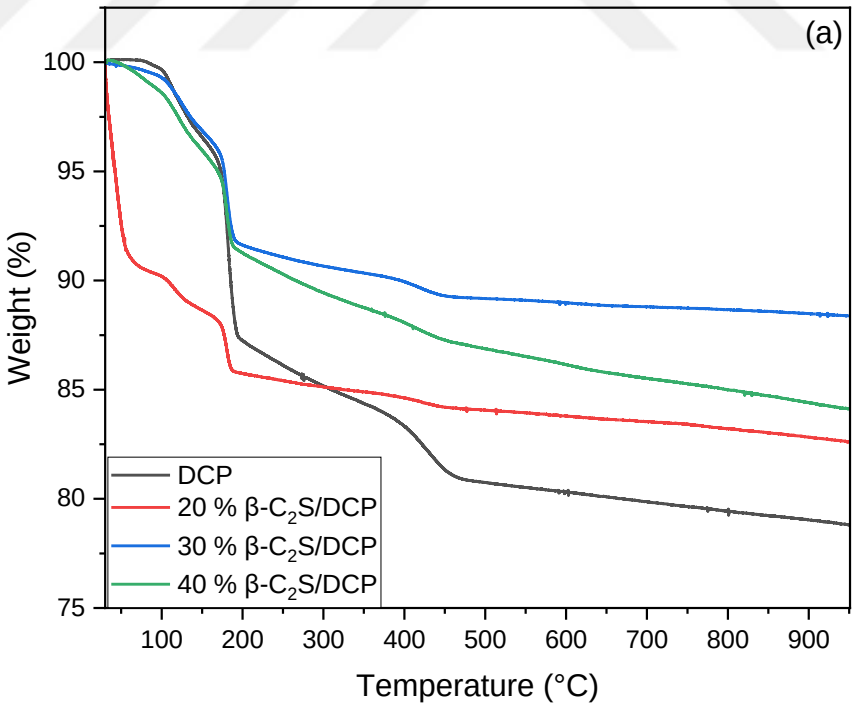

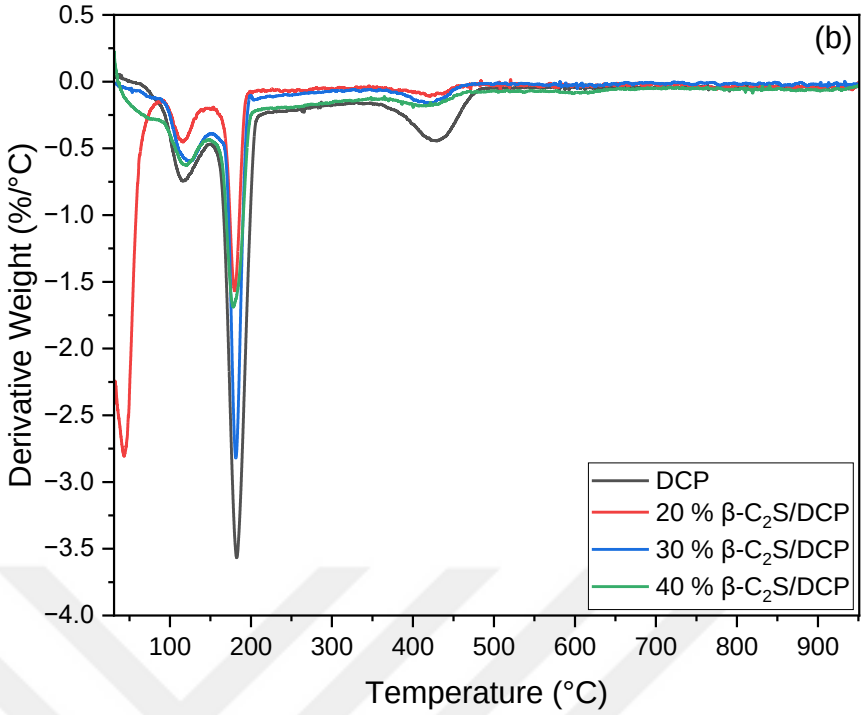

Figure 4.10. Thermograms of pure DCP cement and β-C_2S/ DCP composite cement: (a) TGA, (b) DTA.

Figure 4.11 displays the compressive strength of the prepared cement samples. The pure DCP bone cement exhibited a compressive strength of approximately 0.786 MPa, which aligns with the values reported by Al-Tamimi et al. [74,76]. Incorporating 20% β-C_2S into the cement increased the compressive strength to around 0.925 MPa. This increase is likely due to the transformation of the brushite phase into monetite, which has a lower compressive strength than brushite, as indicated by the measurements. Increasing the proportion of β-C_2S to 30% further elevated the compressive strength to approximately 4.25 MPa. The consolidation of the cement matrix, which significantly influences the microstructural system of the cement, is responsible for this improvement in mechanical properties. The study found that the inclusion of β-C_2S enhanced both the microhardness and compressive strength of DCP cement. Using 40% β-C_2S cement, we achieved a compressive strength of 8.19 MPa. The addition of β-C_2S to DCP cement resulted in a substantial increase in compressive strength, nearly tenfold higher than that of pure DCP cement. According to mechanical investigations, the compressive strength of the β-C_2S/DCP cement combination is comparable to that of human cancellous bone, which ranges between 5 and 10 Mpa [74].

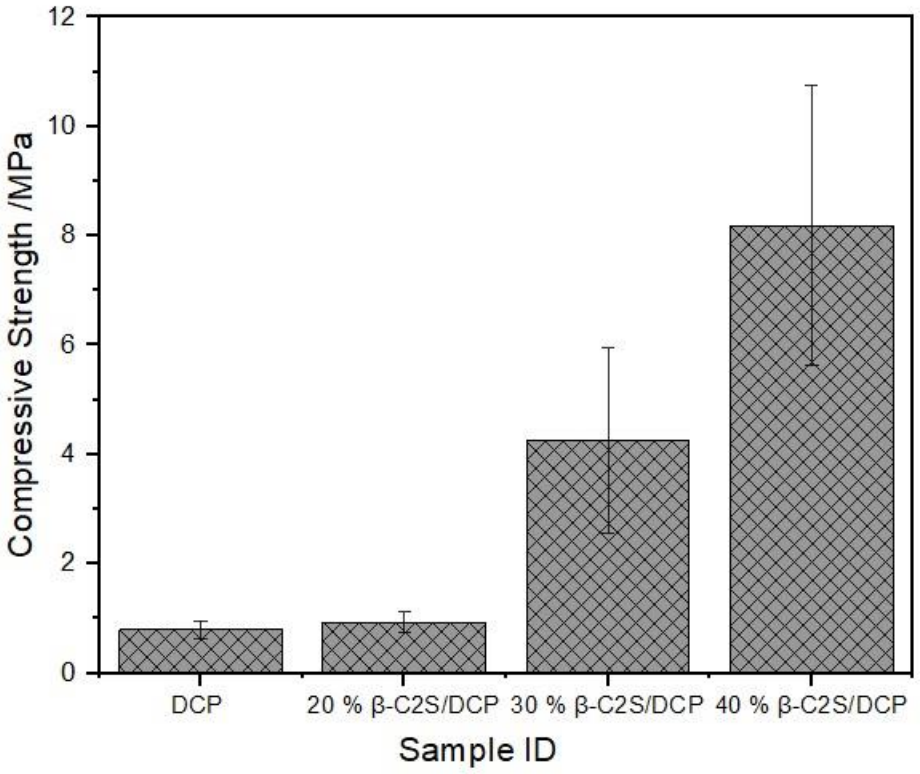

Figure 4.11. Compressive strengths of pure DCP and β-C_2S / DCP scaffolds. The error bars show ± standard deviation.

Figure 4.12 illustrates the effect of pure DCP cement and β-C_2S/DCP composite cement loaded with gentamicin antibiotics on *S. aureus* growth. For the DCP pure sample, the bacterial growth is relatively low across all concentrations. The highest growth is observed with the 0.2 g/mL concentration, reaching approximately 0.1, while other concentrations show negligible growth. In contrast, the 20% β-C_2S/DCP sample exhibits the highest bacterial growth among all tested samples, with the 0.2 g/mL concentration peaking at approximately 0.45. Other concentrations in this sample also show significant bacterial growth, around 0.4. The 30% β-C_2S/DCP sample shows lower bacterial growth than the 20% β-C_2S/DCP sample. The highest growth is observed in the 0.2 g/mL concentration, slightly above 0.3, while other concentrations show growth around 0.25 to 0.3. The 40% β-C_2S/DCP sample displays intermediate bacterial growth. The 0.2 G concentration shows the highest growth, around 0.35, while the 0.1 G concentration shows a significant drop in growth compared to the 0.2 G concentration. Other concentrations in this sample show growth around 0.25. The

controls, PC (Positive Control) and NC (Negative Control), show the expected results. The PC shows a high level of bacterial growth, indicating the expected growth without any inhibitory effect from the cement. In contrast, the NC shows negligible bacterial growth, indicating the absence of contamination or external factors promoting bacterial growth.

At the lowest concentrations (0.00625 g/mL, 0.0125 g/mL, 0.025 g/mL), bacterial growth for pure DCP is minimal, with values close to zero, indicating that even small amounts of DCP are effective in inhibiting bacterial growth. In the 20% β-C_2S/DCP sample, there is still significant bacterial growth at low concentrations, though slightly reduced compared to higher concentrations. For instance, at 0.00625 g/mL, bacterial growth is around 0.3, and at 0.0125 g/mL, it is slightly above 0.3. These values are higher than those observed for pure DCP, suggesting that adding 20% C_2S reduces the antibacterial efficacy of the cement. For the 30% β-C_2S/DCP sample, bacterial growth at the lowest concentrations is also significant but slightly lower than the 20% β-C_2S/DCP sample. For example, at 0.00625 g/mL, growth is around 0.25. At 0.0125 g/mL, it is slightly above 0.25, indicating some improvement in antibacterial properties compared to the 20% β-C_2S/DCP sample but still less effective than pure DCP. At low concentrations, the 40% β-C_2S/DCP sample shows lower bacterial growth compared to the 20% and 30% β-C_2S/DCP samples. For instance, at 0.00625 g/mL, growth is around 0.2. At 0.0125 g/mL, it is slightly above 0.2, suggesting that increasing the β-C_2S content to 40% enhances the antibacterial properties of the composite cement. However, it still does not match the efficacy of pure DCP.

The figure demonstrates that pure DCP cement has the least impact on bacterial growth, while the 20% β-C_2S/DCP composite cement shows the highest bacterial growth. Increasing the percentage of C2S in the composite cement tends to reduce bacterial growth, with the 40% β-C_2S/DCP composite showing intermediate growth levels. The error bars indicate measurement variability, but the trends are clear across different concentrations and compositions. Based on the results, the leaching amount of gentamicin from DCP was higher than other materials, while it was lower for the 20% β-C_2S/DCP composite. This behavior could be attributed to the microstructural properties of the materials. Specifically, DCP cements exhibit a lower degree of

crystallinity, resulting in a higher degradation rate and a higher leaching profile for gentamicin (Table 4.3) [104,121,122,136]. Furthermore, DCP has a unique particle shape, such as a nano-flake-like or layered structure (Figure 4.9), which facilitates the release of the antibiotic [128,129]

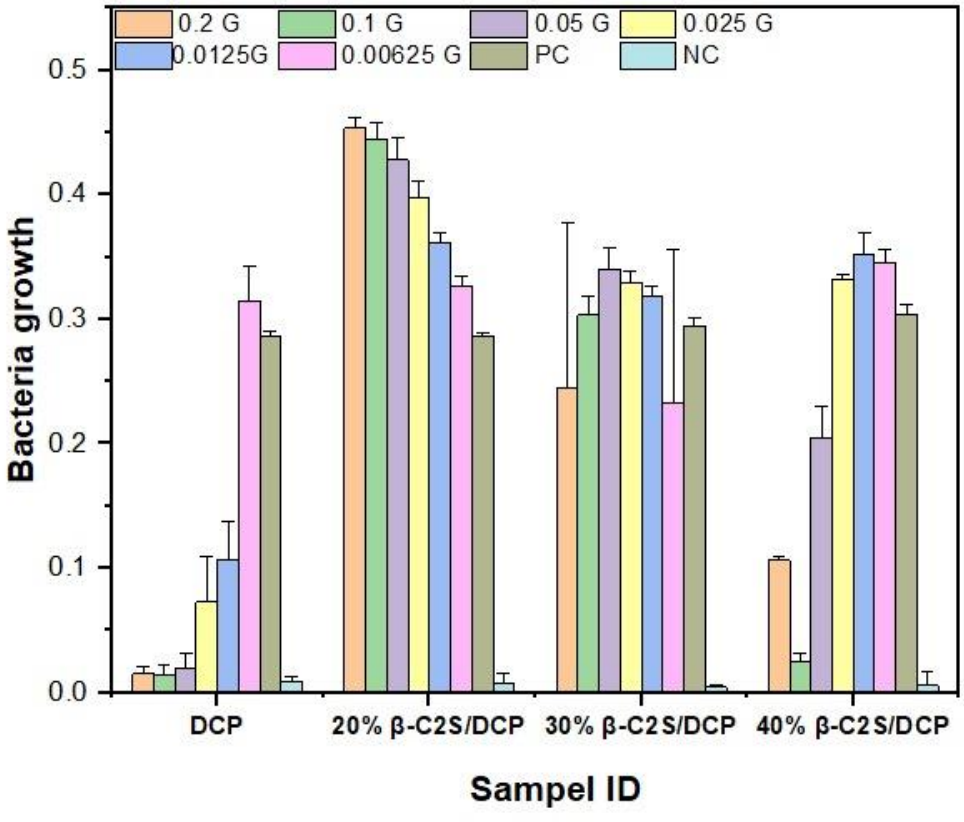

Figure 4.12. Effect of pure DCP cement and β-C_2S / DCP composite cement on S. aureus. The error bars show ± standard deviation. PC: Positive Control, and NC: Negative Control

Figure 4.13 illustrates the fluorescence intensity (measured at 530/590 nm) over time (1, 4, and 7 days) for different cement compositions. The compositions tested include pure DCP cement and β-C_2S/DCP composite cements with varying percentages (20%, 30%, and 40%) of β-C_2S, all loaded with gentamicin. On Day 1, pure DCP cement shows the lowest fluorescence intensity, while the 30% β-C_2S/DCP composite exhibits slightly higher fluorescence than pure DCP. The 20% and 40% β-C_2S/DCP composites display similar fluorescence intensities, both higher than the control group. By Day 4, all samples show an increase in fluorescence intensity compared to Day 1, with the

30% β-C_2S/DCP composite demonstrating the highest fluorescence intensity. The 20% and 40% composites have similar intensities, both surpassing the control group. On Day 7, fluorescence intensity was significantly increased for all samples compared to Day 4. The 20% β-C_2S/DCP composite shows the highest fluorescence intensity, while the 30% and 40% composites have similar intensities, both higher than pure DCP. The error bars, representing the standard deviation, indicate relatively small measurement variability, suggesting consistent results across replicates. Overall, the figure demonstrates that β-C_2S/DCP composite cements support better growth of Saos-2 cells compared to pure DCP cement, with the 20% β-C_2S/DCP composition being the most effective in promoting cell viability.

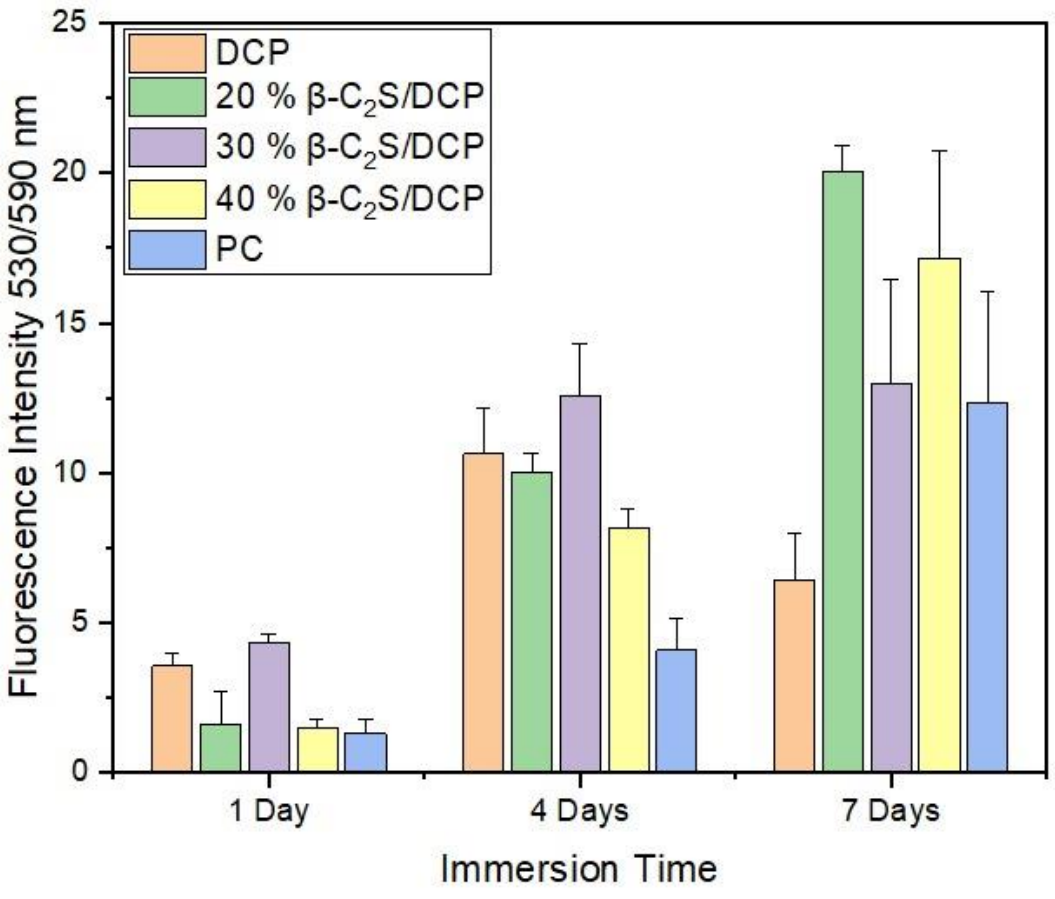

Figure 4.13 Effect of pure DCP cement and β-C_2S/DCP composite cement loaded with gentamicin antibiotic on the growth of Saos-2 cells. The error bars show ± standard deviation

The data suggest that pH levels significantly impact cell viability (Table 4.5). The pure DCP cement, with a pH of 6, supports the least cell growth. The 20% and 40% β-C_2S/DCP composites, both with a pH of 8, support better cell viability than pure DCP but are not as effective as the 30% β-C_2S/DCP composite, which maintains a pH of 7. This indicates that a slightly alkaline environment (pH 7) is more conducive to Saos-2 cell growth compared to a more neutral or highly alkaline environment. Therefore, the pH level plays a crucial role in cell viability, with a pH of 7 being optimal for promoting cell proliferation in these cement compositions.

Table 4.5. The pH changes during the incubation period.

	DAY1	**DAY4**	**DAY7**
pure DCP	6	6	6
20% β-C_2S/DCP	8	8	8
30% β-C_2S/DCP	7	7	7
40% β-C_2S/DCP	8	8	8
Positive Control	8	8	8
Negative Control	8	8	8

CHAPTER 5

CONCLUSION AND RECOMMENDATIONS FOR FUTURE WORKS

5.1. CONCLUSION

The study focused on synthesizing and characterizing β-Dicalcium silicate (β-C_2S) and Dicalcıum phosphate (DCP)-based composite cements for dental and orthopedic applications. B- Tricalcium phosphate (β-TCP) and β-C_2S were successfully synthesized using microwave-assisted wet precipitation and sol-gel methods. XRD analysis confirmed the formation of pure β-TCP and β-C_2S phases, while SEM images revealed spherical β-TCP particles and interconnected β-C_2S particles. FTIR spectra identified characteristic peaks for both materials. The composite cements were prepared by combining DCP with varying amounts of β-C_2S (20%, 30%, and 40%). XRD patterns showed the presence of brushite and monetite phases in the composites, with changes in peak intensity and morphology upon β-C_2S addition. SEM analysis revealed that pure DCP particles had a plate-like structure, while β-C_2S addition resulted in a more cross-linked and fibrous microstructure. FTIR spectra confirmed the presence of various functional groups in the composites. TGA analysis demonstrated improved thermal stability of the composites compared to pure DCP. Compressive strength tests showed that the addition of β-C_2S significantly enhanced the mechanical properties of the cements, with the 40% β-C_2S/DCP composite reaching 8.19 MPa, comparable to human cancellous bone. Antibacterial activity tests against S. aureus revealed that pure DCP cement loaded with gentamicin had the highest antibacterial efficacy, while the 20% β-C_2S/DCP composite showed the least inhibition of bacterial growth. Cytocompatibility studies using Saos-2 cells indicated that the 20% β-C_2S/DCP composite supported the highest cell viability, attributed to its optimal pH level of 7. These results suggest that β-C_2S/DCP composite cements offer a promising balance of mechanical strength, antibacterial activity, and biocompatibility for potential dental applications.

5.2. FUTURE STUDIES

Based on the findings and limitations of this study, the following areas are recommended for future research:

- Investigate the in vitro and in vivo degradation behavior of the β-C_2S/DCP composites over extended periods to understand their long-term stability and resorption characteristics better.
- Conduct a more detailed analysis of β-C_2S concentrations between 30-50% to fine-tune the optimal composition for balancing mechanical properties, antibacterial activity, and biocompatibility.
- Perform animal studies to evaluate the biocompatibility, osseointegration, and bone regeneration capacity of the optimized β-C_2S/DCP composites in real physiological environments.
- Explore the potential of these composites as drug delivery systems by incorporating various therapeutic agents and studying their release profiles.
- Investigate the incorporation of additional reinforcing materials or surface treatments to further improve the mechanical properties of the composites, particularly for load-bearing applications.
- Conduct more in-depth research on the antibacterial mechanisms of the composites and explore ways to maintain strong antibacterial activity while increasing β-C_2S content.
- Evaluate the potential of using these composite materials in 3D printing technologies for creating custom-designed scaffolds or implants.
- Perform head-to-head comparisons with commercially available bone cements to benchmark the performance of these novel β-C_2S/DCP composites.

These future studies will help address current limitations and further develop the potential of β-C_2S/DCP composites for clinical applications in dentistry and orthopedic

REFERENCES

1. Qian, Y., Gong, J., Lu, K., Hong, Y., Zhu, Z., Zhang, J., Zou, Y., Zhou, F., Zhang, C., Zhou, S., Gu, T., Sun, M., Wang, S., He, J., Li, Y., Lin, J., Yuan, Y., Ouyang, H., Yu, M., and Wang, H., "DLP printed hDPSC-loaded GelMA microsphere regenerates dental pulp and repairs spinal cord", ***Biomaterials***, 299, 122137: 1-17 (2023).

2. Samiei, M., Fathi, M., Barar, J., Fathi, N., Amiryaghoubi, N., and Omidi, Y., "Bioactive hydrogel-based scaffolds for the regeneration of dental pulp tissue", ***Journal of Drug Delivery Science and Technology***, 64, 102600: 1-13 (2021).

3. Ahonen, H., Pakpour, A., Norderyd, O., Broström, A., Fransson, E. I., and Lindmark, U., "Applying World Dental Federation Theoretical Framework for Oral Health in a General Population", ***International Dental Journal***, 72 (4): 536–544 (2022).

4. Iftikhar, S., Jahanzeb, N., Saleem, M., ur Rehman, S., Matinlinna, J. P., and Khan, A. S., "The trends of dental biomaterials research and future directions: A mapping review", ***The Saudi dental journal***, 33 (5): 229-238 (2021).

5. Simila, H. O., and Boccaccini, A. R., "Sol-gel bioactive glass containing biomaterials for restorative dentistry: A review", ***Dental Materials***, 38 (5): 725-747 (2022).

6. Rekow, E. D., Fox, C. H., Watson, T., and Petersen, P. E., "Future innovation and research in dental restorative materials", ***Advances In Dental Research***, 25 (1): 1–7 (2013).
7. Montazerian, M., Baino, F., Fiume, E., Migneco, C., Alaghmandfard, A., Sedighi, O., and Mauro, J. C., "Glass-ceramics in dentistry: Fundamentals, technologies, experimental techniques, applications, and open issues", ***Progress in Materials Science***, 132, 101023: 1-88 (2023).

8. Davaie, S., Hooshmand, T., and Ansarifard, S., "Different types of bioceramics as dental pulp capping materials: A systematic review", ***Ceramics International***, 47(15): 20781-20792 (2021).

9. Thein-Han, W., Liu, J., and Xu, H. H. K., "Calcium phosphate cement with biofunctional agents and stem cell seeding for dental and craniofacial bone repair", ***Dental Materials***, 28 (10): 1059–1070 (2012).

10. Yan, H., De Deus, G., Kristoffersen, I. M., Wiig, E., Reseland, J. E., Johnsen, G. F., Silva, E. J. N. L., and Haugen, H. J., "Regenerative endodontics by cell

homing: a review of recent clinical trials", ***Journal of Endodontics***, 49 (1): 4-17 (2023).

11. Habraken, W., Habibovic, P., Epple, M., and Bohner, M., "Calcium phosphates in biomedical applications: materials for the future?", ***Materials today***, 19 (2): 69-87 (2016).

12. Shu, Y., Zhou, Y., Ma, P., Li, C., Ge, C., Wang, Y., Li, Q., Yu, K., Lu, R., Zou, X., Yin, Y., and Li, J., "Degradation in vitro and in vivo of β-TCP/MCPM-based premixed calcium phosphate cement", ***Journal Of The Mechanical Behavior Of Biomedical Materials***, 90: 86–95 (2019).

13. Sarna-Boś, K., Skic, K., Boguta, P., Adamczuk, A., Vodanovic, M., and Chałas, R., "Elemental mapping of human teeth enamel, dentine and cementum in view of their microstructure", ***Micron***, 172, 103485: 1-7 (2023).

14. Sánchez-Enríquez, J. and Reyes-Gasga, J., "Obtaining $Ca(H_2PO_4)_2 \cdot H_2O$, monocalcium phosphate monohydrate, via monetite from brushite by using sonication", ***Ultrasonics Sonochemistry***, 20 (3): 948–954 (2013).

15. Xie, Z., Shen, Z., Zhan, P., Yang, J., Huang, Q., Huang, S., and Lin, Z., "Functional dental pulp regeneration: basic research and clinical translation", ***International journal of molecular sciences***, 22 (16), 8991: 1-27 (2021).

16. Vaishya, R., Chauhan, M., and Vaish, A., "Bone cement", ***Journal of clinical orthopaedics and trauma***, 4 (4): 157-163 (2013).

17. Dohnalík, P., Pichler, B. L. A., Zelaya-Lainez, L., Lahayne, O., Richard, G., and Hellmich, C., "Micromechanics of dental cement paste", ***Journal Of The Mechanical Behavior Of Biomedical Materials***, 124: 1-15 (2021).

18. Raposo, C. C., Nery, L. M. S., Carvalho, E. M., Ferreira, P. V. C., Ardenghi, D. M., Bauer, J., and Lima, D. M.,"Effect of preheating on the physicochemical properties and bond strength of composite resins utilized as dental cements: An in vitro study", ***The Journal of Prosthetic Dentistry***, 129 (1): 1-7 (2023).

19. O'Brien, W. J. (Ed.). "Dental materials and their selection", (Vol. 10). Chicago: Quintessence: 1-10 (2002).

20. Alshemary, A. Z., Bilgin, S., Işık, G., Motameni, A., Tezcaner, A., and Evis, Z., "Biomechanical Evaluation of an Injectable Alginate / Dicalcium Phosphate Cement Composites for Bone Tissue Engineering", ***Journal Of The Mechanical Behavior Of Biomedical Materials***, 118: 1-11 (2021).

21. Unosson, E., Cai, Y., Jiang, X., Lööf, J., Welch, K., and Engqvist, H., "Antibacterial properties of dental luting agents: Potential to hinder the development of secondary caries", ***International Journal Of Dentistry***, 2012(1): 1-7 (2012).

22. AlSahafi, R., Mitwalli, H., Alhussein, A., Melo, M. A. S., Martinho, F., Lynch, C. D., Oates, T. W., Xu, H. H. K., and Weir, M. D., "Novel rechargeable nanostructured calcium phosphate crown cement with long-term ion release and antibacterial activity to suppress saliva microcosm biofilms", ***Journal Of Dentistry***, 122: 1-15 (2022).

23. Tamimi, F., Sheikh, Z., and Barralet, J., "Dicalcium phosphate cements: Brushite and monetite", ***Acta biomaterialia***, 8 (2): 474-487 (2012).

24. Ginebra, M. P., Traykova, T., and Planell, J. A. "Calcium phosphate cements as bone drug delivery systems: a review", ***Journal of controlled release***, 113 (2): 102-110 (2006)..

25. Bohner, M., Gbureck, U., and Barralet, J. E., "Technological issues for the development of more efficient calcium phosphate bone cements: A critical assessment", ***Biomaterials***, 26 (33): 6423–6429 (2005).

26. Wu, B. C., Youn, S. C., Kao, C. T., Huang, S. C., Hung, C. J., Chou, M. Y., Huang, T. H., and Shie, M. Y., "The effects of calcium silicate cement/fibroblast growth factor-2 composite on osteogenesis accelerator in human dental pulp cells", ***Journal Of Dental Sciences***, 10 (2): 145–153 (2015).

27. Maté-Sánchez de Val, J. E., Calvo-Guirado, J. L., Granero Marín, J. M., Gómez Moreno, G., Mazón, P., and de Aza, P. N., "Material characterization and in vivo behavior of dicalcium silicate cement modified with phosphorus", ***Ceramics International***, 42 (1partA): 952–960 (2016).

28. Martínez, I. M., Velásquez, P. A., and De Aza, P. N., "Synthesis and stability of α-tricalcium phosphate doped with dicalcium silicate in the system $Ca_3(PO_4)_2$-Ca_2SiO_4", ***Materials Characterization***, 61 (7): 761–767 (2010).

29. Gou, Z. and Chang, J., "Synthesis and in vitro bioactivity of dicalcium silicate powders", ***Journal Of The European Ceramic Society***, 24 (1): 93–99 (2004).

30. Mohammed, L., Gomaa, H. G., Ragab, D., and Zhu, J. "Magnetic nanoparticles for environmental and biomedical applications: A review", ***Particuology***, 30, 1-14 (2017).

31. Chen, C. C., Shie, M. Y., and Ding, S. J., "Human dental pulp cell responses to new calcium silicate-based endodontic materials", ***International Endodontic Journal***, 44 (9): 836–842 (2011).

32. Gandolfi, M. G., Ciapetti, G., Taddei, P., Perut, F., Tinti, A., Cardoso, M. V., Van Meerbeek, B., and Prati, C., "Apatite formation on bioactive calcium-silicate cements for dentistry affects surface topography and human marrow stromal cells proliferation", ***Dental Materials***, 26 (10): 974–992 (2010).

33. Wu, B. C., Wei, C. K., Hsueh, N. S., and Ding, S. J., "Comparative cell attachment, cytotoxicity and antibacterial activity of radiopaque dicalcium silicate cement and white-coloured mineral trioxide aggregate", ***International Endodontic Journal***, 48 (3): 268–276 (2015).

34. Gou, Z., Chang, J., Zhai, W., and Wang, J., "Study on the self-setting property and the in vitro bioactivity of β-Ca_2SiO_4", ***Journal Of Biomedical Materials Research - Part B Applied Biomaterials***, 73 (2): 244–251 (2005).

35. Chiang, T. Y. and Ding, S. J., "Physicochemical properties of radiopaque dicalcium silicate cement as a root-end filling material in an acidic environment", ***International Endodontic Journal***, 46 (3): 234–241 (2013).

36. Saghiri, M. A., Orangi, J., Asatourian, A., Gutmann, J. L., Garcia-Godoy, F., Lotfi, M., and Sheibani, N., "Calcium silicate-based cements and functional impacts of various constituents", ***Dental materials journal***, 36 (1): 8-18 (2017).

37. Ruiz, J., Moreno, D., Copete, H., Vargas, F., and López, M. E., "Calcium phosphate cements improved by addition of carbonated Hydroxyapatite type B", ***Boletin De La Sociedad Espanola De Ceramica Y Vidrio***, *62*(4): 315-328 (2022).

38. Bohner, M., "Resorbable biomaterials as bone graft substitutes", ***Materials Today***, 13 (1-2): 24-30 (2010).

39. Dorozhkin, S. V. , "A history of calcium orthophosphates ($CaPO_4$) and their biomedical applications", ***Morphologie***, 101 (334): 143-153 (2017).

40. Prihanto, A., Fitriyana, D. F., Muryanto, S., Masykur, I., Ismail, R., Jamari, J., and Bayuseno, A. P., "Aqueous crystallization of monocalcium phosphate monohydrate with green mussel shells (Verna piridis) for calcium sources", ***Journal Of Environmental Chemical Engineering***, 9 (6): 1-9 (2021).

41. Huang, C. and Cao, P., "Tuning Ca:P ratio by NaOH from monocalcium phosphate monohydrate (MCPM)", ***Materials Chemistry And Physics***, 181: 159–166 (2016).

42. Dorozhkin, S. V. Calcium orthophosphates in nature, biology and medicine. *Materials*, *2*(2): 399-498 (2009).

43. Taha, A., Akram, M., Jawad, Z., Alshemary, A. Z., and Hussain, R., "Strontium doped injectable bone cement for potential drug delivery applications", ***Materials Science And Engineering C***, 80: 93–101 (2017).

44. Sivaraj, D., Arumugam, G., Kalimuthu, V., and Rajendran, R., "Enhanced anti-biofilm and biocompatibility of Zn and Mg substituted β-tricalcium phosphate/functionalized multiwalled carbon nanotube composites towards A. baumannii and Methicillin-Resistant Staphylococcus aureus, and MG-63 cells", ***International Journal Of Pharmaceutics***, 627: 1-10 (2022).

45. Bagherifard, A., Joneidi Yekta, H., Akbari Aghdam, H., Motififard, M., Sanatizadeh, E., Ghadiri Nejad, M., and Khandan, A., "Improvement in osseointegration of tricalcium phosphate-zircon for orthopedic applications: an in vitro and in vivo evaluation", ***Medical & biological engineering & computing***, 58: 1681-1693 (2020).

46. Moreno, D., Vargas, F., Ruiz, J., and López, M. E., "Solid-state synthesis of alpha tricalcium phosphate for cements used in biomedical applications", ***Boletin De La Sociedad Espanola De Ceramica Y Vidrio***, 59 (5): 193–200 (2020).

47. Sinusaite, L., Renner, A. M., Schütz, M. B., Antuzevics, A., Rogulis, U., Grigoraviciute-Puroniene, I., Mathur, S., and Zarkov, A., "Effect of Mn doping on the low-temperature synthesis of tricalcium phosphate (TCP) polymorphs", ***Journal Of The European Ceramic Society***, 39 (10): 3257–3263 (2019).

48. Carrodeguas, R. G., and De Aza, S., "α-Tricalcium phosphate: Synthesis, properties and biomedical applications", ***Acta biomaterialia***, 7 (10): 3536-3546 (2011).

49. Bohner, M., Santoni, B. L. G., and Döbelin, N., "β-tricalcium phosphate for bone substitution: Synthesis and properties", ***Acta biomaterialia***, 113: 23-41 (2020).

50. Somers, N., Jean, F., Lasgorceix, M., Preux, N., Delmotte, C., Boilet, L., Petit, F., and Leriche, A., "Fabrication of doped β-tricalcium phosphate bioceramics by Direct Ink Writing for bone repair applications", ***Journal Of The European Ceramic Society***, 43 (2): 629–638 (2023).

51. Mandić, V., Radovanović-Perić, F., Panžić, I., and Vrsaljko, D., "Addressing of different synthetic and shaping approaches for β-tri calcium phosphate macro-microporous scaffold fabrication", ***Ceramics International***, 49 (9): 14934–14940 (2023).

52. Wu, Y., Zhang, S., Sun, L., Lu, Y., Jiang, Y., and Xiao, G., "Strontium doping stimulates the phase composition and evolution of β-tricalcium phosphate prepared by wet chemical method", ***Journal Of Solid State Chemistry***, 318: 1-9 (2023).

53. Djošić, M. S., Mišković-Stanković, V. B., Milonjić, S., Kačarević-Popović, Z. M., Bibić, N., and Stojanović, J., "Electrochemical synthesis and characterization of hydroxyapatite powders", ***Materials Chemistry And Physics***, 111 (1): 137–142 (2008).

54. Huang, A., Dai, H., Wu, X., Zhao, Z., and Wu, Y., "Synthesis and characterization of mesoporous hydroxyapatite powder by microemulsion technique", ***Journal Of Materials Research And Technology***, 8 (3): 3158–3166 (2019).

55. Ruiz-Aguilar, C., Olivares-Pinto, U., Aguilar-Reyes, E. A., López-Juárez, R., and Alfonso, I., "Characterization of β-tricalcium phosphate powders synthesized by sol-gel and mechanosynthesis", ***Boletin De La Sociedad Espanola De Ceramica Y Vidrio***, 57 (5): 213–220 (2018).

56. Krauklis, A. E., Kreicbergs, I., and Dreyer, I., "Modified ginstling–brounshtein model for wet precipitation synthesis of hydroxyapatite: Analytical and experimental study", ***Acta Of Bioengineering And Biomechanics***, 20 (4): 47–57 (2018).

57. Lee, D. S. H., Pai, Y., and Chang, S., "Effect of pH control of mixture solution on the fabrication of the highly pure β-tricalcium phosphate powders synthesized by liquid-solid mixture precipitation method", ***Materials Letters***, 102–103: 76–79 (2013).

58. Lee, J. H., Chang, B. S., Jeung, U. O., Park, K. W., Kim, M. S., and Lee, C. K., "The first clinical trial of beta-calcium pyrophosphate as a novel bone graft extender in instrumented posterolateral Lumbar fusion", ***Clinics In Orthopedic Surgery***, 3 (3): 238–244 (2011).

59. Kim, I. S. and Kumta, P. N., "Sol-gel synthesis and characterization of nanostructured hydroxyapatite powder", ***Materials Science And Engineering B: Solid-State Materials For Advanced Technology***, 111 (2–3): 232–236 (2004).

60. He, S. and Xu, Y., "Hydrothermal-assisted solid-state reaction synthesis of high ionic conductivity $Li_{1+X}Al_XTi_{2-X}(PO_4)_3$ ceramic solid electrolytes: The effect of Al^{3+} doping content", ***Solid State Ionics***, 343: 1-8 (2019).

61. Sanosh, K. P., Chu, M. C., Balakrishnan, A., Kim, T. N., and Cho, S. J., "Sol-gel synthesis of pure nano sized β-tricalcium phosphate crystalline powders", ***Current Applied Physics***, 10 (1): 68–71 (2010).

62. Aurobind, S. V., Amirthalingam, K. P., and Gomathi, H., "Sol-gel based surface modification of electrodes for electro analysis", ***Advances in colloid and interface science***, 121 (1-3): 1-7 (2006).

63. Peng, S. Y., Lin, Y. W., Lin, Y. Y., and Lin, K. L., "Hydrothermal synthesis of hydroxyapatite nanocrystals from calcium-rich limestone sludge waste: Preparation, characterization, and application for Pb^{2+} adsorption in aqueous solution", ***Inorganic Chemistry Communications***, 160: 1-14 (2023).

64. Bensalah, H., Bekheet, M. F., Alami Younssi, S., Ouammou, M., and Gurlo, A., "Hydrothermal synthesis of nanocrystalline hydroxyapatite from phosphogypsum waste", ***Journal Of Environmental Chemical Engineering***, 6 (1): 1347–1352 (2018).

65. Zhang, X. and Vecchio, K. S., "Hydrothermal synthesis of hydroxyapatite rods", ***Journal Of Crystal Growth***, 308 (1): 133–140 (2007).

66. Guo, X. and Xiao, P., "Effects of solvents on properties of nanocrystalline hydroxyapatite produced from hydrothermal process", ***Journal Of The European Ceramic Society***, 26 (15): 3383–3391 (2006).

67. Byrappa, K., and Adschiri, T., "Hydrothermal technology for nanotechnology", ***Progress in crystal growth and characterization of materials***, 53 (2): 117-166 (2007).

68. Sha, L., Liu, Y., Zhang, Q., Hu, M., and Jiang, Y., "Microwave-assisted co-precipitation synthesis of high purity β-tricalcium phosphate crystalline powders", ***Materials Chemistry And Physics***, 129 (3): 1138–1141 (2011).

69. Saleh, T. A., Majeed, S., Nayak, A., and Bhushan, B., "Principles and advantages of microwave- assisted methods for the synthesis of nanomaterials for water purification", Advanced Nanomaterials for Water Engineering, Treatment, and Hydraulics, ***IGI Global***, 40–57 (2017).

70. Shavandi, A., Alaa, A. E. D., Ali, A., Sun, Z., and Ratnayake, J. T., "Microwave-assisted synthesis of high purity β-tricalcium phosphate crystalline powder from the waste of Green mussel shells (Perna canaliculus)", ***Powder Technology***, 273: 33–39 (2015).

71. Webler, G. D., Zapata, M. J. M., Agra, L. C., Barreto, E., Silva, A. O. S., Hickmann, J. M., and Fonseca, E. J. S., "Characterization and evaluation of cytotoxicity of biphasic calcium phosphate synthesized by a solid state reaction route", ***Current Applied Physics***, 14 (6): 876–880 (2014).

72. Punj, S., Singh, J., and Singh, K. J. C. I., "Ceramic biomaterials: Properties, state of the art and future prospectives", ***Ceramics International***, 47 (20), 28059-28074 (2021).

73. El Hazzat, M., El Hamidi, A., Halim, M., and Arsalane, S., "Complex evolution of phase during the thermal investigation of Brushite-type calcium phosphate $CaHPO_4.2H_2O$", ***Materialia***, 16: 1-8 (2021).

74. Motameni, A., Alshemary, A. Z., Dalgic, A. D., Keskin, D., and Evis, Z., "Lanthanum doped dicalcium phosphate bone cements for potential use as filler for bone defects", ***Materials Today Communications***, 26: 1-10 (2021).

75. Qadir, M. A., Ahmed, M. A. H. M. O. O. D., Ahmed, S., and Ul-Haq, I., "Synthesis of Dicalcium Phosphate Used as Feed Additive for Animals From Phosphate Rock as Potential Cost-Effective Raw Material", ***International Journal of Chemical Sciences***, 12 (1): 111-120 (2014).

76. Tamimi, F., Nihouannen, D. Le, Eimar, H., Sheikh, Z., Komarova, S., and Barralet, J., "The effect of autoclaving on the physical and biological properties of dicalcium phosphate dihydrate bioceramics: Brushite vs. monetite", ***Acta Biomaterialia***, 8 (8): 3161–3169 (2012).

77. Tamimi, F., Nihouannen, D. Le, Eimar, H., Sheikh, Z., Komarova, S., and Barralet, J., "The effect of autoclaving on the physical and biological properties of dicalcium phosphate dihydrate bioceramics: Brushite vs. monetite", ***Acta Biomaterialia***, 8 (8): 3161–3169 (2012).

78. Tamimi, F., Torres, J., Bettini, R., Ruggera, F., Rueda, C., López-Ponce, M., and Lopez-Cabarcos, E., "Doxycycline sustained release from brushite cements for the treatment of periodontal diseases", ***Journal Of Biomedical Materials Research - Part A***, 85 (3): 707–714 (2008).

79. Tamimi, F., Torres, J., Lopez-Cabarcos, E., Bassett, D. C., Habibovic, P., Luceron, E., and Barralet, J. E., "Minimally invasive maxillofacial vertical bone augmentation using brushite based cements", ***Biomaterials***, 30 (2): 208–216 (2009).

80. Fomin, A. S., Fadeeva, I. V., Filippov, Y. Y., Kovalkov, V. K., Grigoryeva, M. A., Shvorneva, L. I., and Barinov, S. M., "Brushite cement based on β-TCP for orthopedics", ***Inorganic Materials: Applied Research***, 8 (2): 292–295 (2017).

81. Ji, C. and Ahn, J. G., "Clinical experience of the brushite calcium phosphate cement for the repair and augmentation of surgically induced cranial defects following the pterional craniotomy", ***Journal Of Korean Neurosurgical Society***, 47 (3): 180–184 (2010).

82. Garskaite, E., Balciunas, G., Drienovsky, M., Sokol, D., Sandberg, D., Bastos, A. C., and Salak, A. N., "Brushite mineralised Scots pine (Pinus sylvestris L.) sapwood - revealing mineral crystallization within a wood matrix by in situ XRD", ***RSC Advances***, 13 (9): 5813–5825 (2023).

83. Mathew, M., and Takagi, S., "Structures of biological minerals in dental research", ***Journal of Research of the National Institute of Standards and Technology***, 106 (6): 1035 (2001).

84. Unosson, J. E., Persson, C., and Engqvist, H., "An evaluation of methods to determine the porosity of calcium phosphate cements", ***Journal Of Biomedical Materials Research - Part B Applied Biomaterials***, 103 (1): 62–71 (2015).

85. Frost, R. L. and Palmer, S. J., "Thermal stability of the “cave” mineral brushite $CaHPO_4 \cdot 2H_2O$ - Mechanism of formation and decomposition", ***Thermochimica Acta***, 521 (1–2): 14–17 (2011).

86. Ghina Imaniyyah, A., Sunarso, and Herda, E., "Monetite as a potential ideal bone substitute: A short review on fabrication and properties", ***Materials Today: Proceedings***, 66: 2762–2766 (2022).

87. Motameni, A., Alshemary, A. Z., and Evis, Z. "A review of synthesis methods, properties and use of monetite cements as filler for bone defects", ***Ceramics International***, 47 (10): 13245-13256 (2021).

88. Koju, N., Sikder, P., Gaihre, B., and Bhaduri, S. B., "Smart injectable self-setting monetite based bioceramics for orthopedic applications", ***Materials***, 11 (7): 1-18 (2018).

89. Tamimi, F., Torres, J., Gbureck, U., Lopez-Cabarcos, E., Bassett, D. C., Alkhraisat, M. H., and Barralet, J. E., "Craniofacial vertical bone augmentation: A comparison between 3D printed monolithic monetite blocks and autologous onlay grafts in the rabbit", ***Biomaterials***, 30 (31): 6318–6326 (2009).

90. Briak, H. El, Durand, D., Nurit, J., Munier, S., Pauvert, B., and Boudeville, P., "Study of a hydraulic dicalcium phosphate dihydrate/calcium oxide-based cement for dental applications", 63 (4): 447-453 (2002).

91. Dorozhkin, S. V., "Calcium orthophosphates", ***Journal Of Materials Science***, 42 (4): 1061–1095 (2007).

92. Tamimi, F., Torres, J., Bassett, D., Barralet, J., and Cabarcos, E. L., "Resorption of monetite granules in alveolar bone defects in human patients", ***Biomaterials***, 31 (10): 2762–2769 (2010).

93. Klammert, U., Reuther, T., Jahn, C., Kraski, B., Kübler, A. C., and Gbureck, U., "Cytocompatibility of brushite and monetite cell culture scaffolds made by three-dimensional powder printing", ***Acta Biomaterialia***, 5 (2): 727–734 (2009).

94. Ruolan, W., Liangjiao, C., and Longquan, S., "The mTOR/ULK1 signaling pathway mediates the autophagy-promoting and osteogenic effects of dicalcium silicate nanoparticles", ***Journal Of Nanobiotechnology***, 18 (1): 1-19 (2020).

95. Chen, L., Zhang, Y., Liu, J., Wei, L., Song, B., and Shao, L., "Exposure of the murine RAW 264.7 macrophage cell line to dicalcium silicate coating: assessment of cytotoxicity and pro-inflammatory effects", ***Journal Of Materials Science: Materials In Medicine***, 27 (3): 1–11 (2016).

96. Correa, D., Almirall, A., García-Carrodeguas, R., Alberto Dos Santos, L., De Aza, A. H., Parra, J., and Ángel Delgado, J., "β-Dicalcium silicate-based cement: Synthesis, characterization and in vitro bioactivity and biocompatibility studies", ***Journal Of Biomedical Materials Research - Part A***, 102 (10): 3693–3703 (2014).

97. Lai, S., Chen, L., Cao, W., Cui, S., Li, X., Zhong, W., Ma, M., and Zhang, Q., "Dicalcium silicate induced proinflammatory responses through TLR2-mediated NF-κB and JNK pathways in the murine RAW 264.7 macrophage cell line", ***Mediators Of Inflammation***, 2018 (1): 1-16 (2018).

98. Liu, W., Huan, Z., Xing, M., Tian, T., Xia, W., Wu, C., Zhou, Z., and Chang, J., "Strontium-substituted dicalcium silicate bone cements with enhanced osteogenesis potential for orthopaedic applications", ***Materials***, 12 (14): 1-16 (2019).

99. Radwan, M. M., Abd El-Hamid, H. K., and Mohamed, A. F., "Influence of saline solution on hydration behavior of β-dicalcium silicate in comparison with biphasic calcium phosphate/hydroxyapatite bio-ceramics", ***Materials Science And Engineering C***, 57: 355–362 (2015).

100. Gou, Z., Chang, J., Zhai, W., and Wang, J., "Study on the self-setting property and the in vitro bioactivity of β-Ca_2SiO_4", ***Journal Of Biomedical Materials Research - Part B Applied Biomaterials***, 73 (2): 244–251 (2005).

101. Chen, C. C., Wang, C. W., Hsueh, N. S., and Ding, S. J., "Improvement of in vitro physicochemical properties and osteogenic activity of calcium sulfate cement for bone repair by dicalcium silicate", ***Journal Of Alloys And Compounds***, 585: 25–31 (2014).

102. Correa, D., Almirall, A., García-Carrodeguas, R., Alberto Dos Santos, L., De Aza, A. H., Parra, J., and Ángel Delgado, J., "β-Dicalcium silicate-based cement: Synthesis, characterization and in vitro bioactivity and biocompatibility studies", ***Journal Of Biomedical Materials Research - Part A***, 102 (10): 3693–3703 (2014).

103. Świeczko-Żurek, B., Zieliński, A., Bociąga, D., Rosińska, K., and Gajowiec, G., "Influence of Different Nanometals Implemented in PMMA Bone Cement on Biological and Mechanical Properties", ***Nanomaterials***, 12 (5): 1-17 (2022).

104. Huan, Z. and Chang, J., "Novel bioactive composite bone cements based on the β-tricalcium phosphate-monocalcium phosphate monohydrate composite cement system", ***Acta Biomaterialia***, 5 (4): 1253–1264 (2009).

105. Reller, L. B., Weinstein, M., Jorgensen, J. H., and Ferraro, M. J., "Antimicrobial susceptibility testing: a review of general principles and contemporary practices", ***Clinical infectious diseases***, 49 (11): 1749-1755 (2009).

106. Grigoraviciute-Puroniene, I., Tsuru, K., Garskaite, E., Stankeviciute, Z., Beganskiene, A., Ishikawa, K., and Kareiva, A., "A novel wet polymeric precipitation synthesis method for monophasic β-TCP", ***Advanced Powder Technology***, 28 (9): 2325–2331 (2017).

107. Taha, A., Akram, M., Jawad, Z., Alshemary, A. Z., and Hussain, R., "Strontium doped injectable bone cement for potential drug delivery applications", ***Materials Science And Engineering C***, 80: 93–101 (2017).

108. Reller, L. B., Weinstein, M., Jorgensen, J. H., and Ferraro, M. J., "Antimicrobial susceptibility testing: a review of general principles and contemporary practices", ***Clinical infectious diseases***, 49 (11): 1749-1755 (2009).

109. Yao, C., Pripatnanont, P., Zhang, J., and Suttapreyasri, S., "Fabrication and characterization of a bioactive composite scaffold based on polymeric collagen/gelatin/nano β-TCP for alveolar bone regeneration", ***Journal Of The Mechanical Behavior Of Biomedical Materials***, 153: 1-12 (2024).

110. Coelho, P. G., Coimbra, M. E., Ribeiro, C., Fancio, E., Higa, O., Suzuki, M., and Marincola, M., "Physico/chemical characterization and preliminary human histology assessment of a β-TCP particulate material for bone augmentation", ***Materials Science And Engineering C***, 29 (7): 2085–2091 (2009).

111. Massit, A., El Yacoubi, A., Hmamouchi, S., Rkhaila, A., Boulouiz, A., Ounine, K., and El Idrissi, B. C., "Sulphate-substituted tricalcium phosphate β-TCP: Effect of SO_4^{-2} insertion and microwave conditions", ***Materials Today: Proceedings***, 72: 3544–3549 (2023).

112. Xie, L., Yu, H., Deng, Y., Yang, W., Liao, L., and Long, Q., "Preparation, characterization and in vitro dissolution behavior of porous biphasic α/β-tricalcium phosphate bioceramics", ***Materials Science And Engineering C***, 59: 1007–1015 (2016).

113. Raynaud, S., Champion, E., Bernache-Assollant, D., and Thomas, P., "Calcium phosphate apatites with variable Ca/P atomic ratio I. Synthesis, characterisation and thermal stability of powders", ***Biomaterials***, *23* (4): 1065-1072 (2002).

114. Mirjalili, F., Mohammadi, H., Azimi, M., Hafezi, M., and Abu Osman, N. A., "Synthesis and characterization of β-TCP/CNT nanocomposite: Morphology, microstructure and in vitro bioactivity", ***Ceramics International***, 43 (10): 7573–7580 (2017).

115. Su, Z., Li, L., Liu, Z., Huang, C., Wang, D., and Wang, T., "Fabrication, microstructure, and hydration of nano β-Ca_2SiO_4 powder by co-precipitation method", ***Construction and Building Materials***, *296*, 123737: 1-9 (2021).

116. Gou, Z. and Chang, J., "Synthesis and in vitro bioactivity of dicalcium silicate powders", ***Journal Of The European Ceramic Society***, 24 (1): 93–99 (2004).

117. Timón, V., Torrens-Martin, D., Fernández-Carrasco, L. J., and Martínez-Ramírez, S., "Infrared and Raman vibrational modelling of β-C_2S and C_3S compounds", ***Cement And Concrete Research***, 169: 1-11 (2023).

118. Yunus, S. N. H., Fhan, K. S., Johar, B., Adzali, N. M. S., Jakfar, N. H., Meng, C. E., and Talib, Z. A., "Formation of Bio-based Derived Dicalcium Silicate Ceramics via Mechanochemical Treatment: Physical, XRD, SEM and FTIR Analyses", ***International Journal of Nanoelectronics & Materials***, 16 (3): 1-19 (2023).

119. Chrysafi, R., Perraki, T., and Kakali, G., "Sol-gel preparation of $2CaO{\cdot}SiO_2$", ***Journal Of The European Ceramic Society***, 27 (2–3): 1707–1710 (2007).

120. Hamdan Alkhraisat, M., Tamimi Mariño, F., Rubio Retama, J., Blanco Jerez, L., and López-Cabarcos, E., "Beta-tricalcium phosphate release from brushite cement surface", ***Journal Of Biomedical Materials Research - Part A***, 84 (3): 710–717 (2008).

121. De Aza, P. N., García-Bernal, D., Cragnolini, F., Velasquez, P., and Meseguer-Olmo, L., "The effects of Ca_2SiO_4-$Ca_3(PO_4)_2$ ceramics on adult human mesenchymal stem cell viability, adhesion, proliferation, differentiation and function", ***Materials Science And Engineering C***, 33 (7): 4009–4020 (2013).

122. Martínez, I. M., Velásquez, P. A., and De Aza, P. N., "Synthesis and stability of α-tricalcium phosphate doped with dicalcium silicate in the system $Ca_3(PO_4)_2$-Ca_2SiO_4", ***Materials Characterization***, 61 (7): 761–767 (2010).

123. Mostafa, N. Y., Kishar, E. A., and Abo-El-Enein, S. A., "FTIR study and cation exchange capacity of Fe^{3+} and Mg^{2+} substituted calcium silicate hydrates", ***Journal Of Alloys And Compounds***, 473 (1–2): 538–542 (2009).

124. Ahmed, M. J., Lambrechts, K., Ling, X., Schollbach, K., and Brouwers, H. J. H., "Effect of hydroxide, carbonate, and sulphate anions on the β-dicalcium silicate hydration rate", ***Cement And Concrete Research***, 173: 1-10 (2023).

125. Mhla, E. and Koutsoukos, P. G., "Heterogeneous crystallization of calcium hydrogen phosphate anhydrous (monetite)", ***Colloids And Surfaces A: Physicochemical And Engineering Aspects***, 513: 125–135 (2017).

126. Joseph, A., Awadh, Z., Dashti, D., and Chakkamalayath, J., "Effect of Superabsorbent Polymer on the Hydration Properties of High-Performance Concrete", 12 (2): 1-5 (2023).

127. Liu, S., Dou, Z., Zhang, S., Zhang, H., Guan, X., Feng, C., and Zhang, J., "Effect of sodium hydroxide on the carbonation behavior of β-dicalcium silicate", ***Construction And Building Materials***, 150: 591–594 (2017).

128. Sridhar, T. M., "Nanobioceramic coatings for biomedical applications", ***Materials Technology***, 25 (3–4): 184–195 (2010).

129. Tas, A. C., "Monetite ($CaHPO_4$) synthesis in ethanol at room temperature", ***Journal Of The American Ceramic Society***, 92 (12): 2907–2912 (2009).

130. Sheikh, Z., Zhang, Y. L., Grover, L., Merle, G. E., Tamimi, F., and Barralet, J., "In vitro degradation and in vivo resorption of dicalcium phosphate cement based grafts", ***Acta biomaterialia***, *26*: 338-346 (2015).

131. Radwan, M. M., Abd El-Hamid, H. K., and Mohamed, A. F., "Influence of saline solution on hydration behavior of β-dicalcium silicate in comparison with biphasic calcium phosphate/hydroxyapatite bio-ceramics", ***Materials Science And Engineering C***, 57: 355–362 (2015).

132. El-Hamid, H. K. A., Abo-Naf, S. M., and Elwan, R. L., "Characterization, bioactivity investigation and cytotoxicity of borosilicate glass/dicalcium silicate composites", ***Journal Of Non-Crystalline Solids***, 512: 25–32 (2019).

133. Alshemary, A. Z., Goh, Y. F., Akram, M., Razali, I. R., Abdul Kadir, M. R., and Hussain, R., "Microwave assisted synthesis of nano sized sulphate doped hydroxyapatite", ***Materials Research Bulletin***, 48 (6): 2106–2110 (2013).

134. Suryawanshi, V. B. and Chaudhari, R. T., "Growth and Characterization of Agar Gel Grown Brushite Crystals", ***Indian Journal Of Materials Science***, 2014: 1–6 (2014).

135. Santillán-Urquiza, E., Arteaga-Cardona, F., Hernandez-Herman, E., Pacheco-García, P. F., González-Rodríguez, R., Coffer, J. L., and Méndez-Rojas, M. A., "Inulin as a novel biocompatible coating: evaluation of surface affinities toward $CaHPO_4$, α-Fe_2O_3, ZnO, $CaHPO_4$@ ZnO and α-Fe_2O_3@ ZnO nanoparticles", ***Journal of colloid and interface science***, *460*: 339-348 (2015).

136. Goh, Y. F., Alshemary, A. Z., Akram, M., Abdul Kadir, M. R., and Hussain, R., "In-vitro characterization of antibacterial bioactive glass containing ceria", ***Ceramics International***, 40 (1 PART A): 729–737 (2014).

RESUME

Almataz Bellah MARANDI graduated from the University of Damascus, Faculty of Engineering, Department of Chemical Engineering in Aleppo in 2020. The master's program at Karabük University, Department of Biomedical Engineering, began in 2021.